Study of Hot Tearing in Cast and Wrought Aluminum Alloys

by

Qinxin Wu

A thesis submitted to the faculty of the

WORCESTER POLYTECHINC INSTITUTE

in partial fulfillment of the requirements of the degree of

Master of Science

in

Materials Process Engineering

August, 2012

Professor Diran Apelian, Advisor

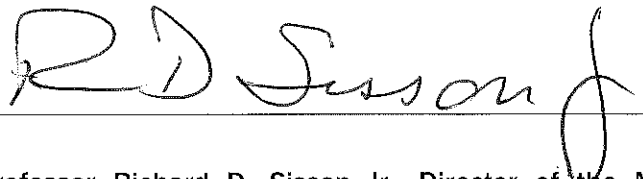

Professor Richard D. Sisson Jr., Director of the Material Science and Engineering Program

Study of Hot Tearing in Cast and Wrought Aluminum Alloys

by

Qinxin Wu

A thesis submitted to the faculty of the

WORCESTER POLYTECHINC INSTITUTE

in partial fulfillment of the requirements of the degree of

Master of Science

in

Materials Process Engineering

August, 2012

Professor Diran Apelian, Advisor

Professor Richard D. Sisson Jr., Director of the Material Science and Engineering Program

ABSTRACT

During the solidification process in casting, hot tearing may occur. It is a severe defect that normally involves the formation of a macroscopic tear, which generates cracks either on the surface or inside the casting. Over the past decades, many strategies have been developed to evaluate the hot tearing tendency. Unfortunately, most of the tests can only provide qualitative information. Therefore, a reliable and quantitative test to evaluate hot tearing in aluminum alloys is highly desirable. To address this issue, WPI and CANMET MTL (both members of the Light Metal Alliance) jointly developed a quantitative hot tearing test and established a specific methodology. Using a constrained rod mold, the hot tearing formation can be quantitatively studied by measuring the contraction force, time and temperature during solidification for a restrained casting or linear contraction, time and temperature for a relaxed casting. This study investigated cast aluminum alloys A380.1 and A390 and wrought aluminum alloys 6061 and 7075. The results show that wrought aluminum alloys have a much stronger hot tearing tendency than cast aluminum alloys based on a quantitative analysis. Also, the study involves the effects of adding strontium and oxides respectively into the cast aluminum alloy A380.1. Compared with the pure A380.1 alloy, the introduction of strontium decreases the hot tearing tendency, while the inclusion of oxide greatly increases the hot tearing. The information obtained through these tests provides a database of hot tearing phenomenon and establishes a new hot tearing index.

ACKNOWLEDGEMENTS

First of all, I would like to thank my advisor Professor Diran Apelian for giving me the opportunity to work with him on this project. He taught me how to approach scientific research. He has been a great help not only in my academic performance, but also in my personal development.

I want to thank Shimin Li for her previous studies on this project and the incredible help in my experiments. I am especially grateful for her time, assistance, and technical knowledge of hot tearing.

I would like to thank Professor Libo Wang for his help in my experiments and encouragement of my topic. Without his help, I would not have been able to complete this thesis on time.

I want to express my gratitude to Professor Richard D. Sisson, Jr. for all of his assistance and suggestions during my study in WPI.

I would also like to thank Carol Garofoli, Maureen Plunkett and Rita Shilansky for all of their time and support in this project. Thanks to all my friends for their understanding and help.

Finally, I would like to thank my parents that always supported me and that never stopped believing in me. Their unconditional love has been an endless source of encouragement throughout my life.

Contents

1. Introduction

Aluminum castings have played an important role in the aluminum industry since the 19th century. Today, aluminum alloy castings are manufactured with a diversity of compositions by various commercial casting processes. However, during solidification hot tearing may occur, which is unacceptable from a quality point of view [1]. Hot tearing involves the formation of a macroscopic tear, which produces cracks either on the surface or inside the casting [2]. Since the 1920s, a number of theories have been developed to explain the hot tearing phenomenon. It is generally believed that hot tearing is related to insufficient liquid feeding to compensate shrinkage during solidification. Hot tearing is influenced by various factors, such as alloy chemistry, volume fraction eutectic in the alloy, freezing range, grain size, grain morphology and processing parameters (such as mold temperature or superheat); it is a complex phenomenon and unfortunately the literature has many contradictions[3].

An important principle in materials processing is that one cannot control what one does not measure. In this vein, there have been many attempts in the past to develop methods and tests to measure hot tearing during solidification. Previous attempts have been based on qualitative "measures" rather than quantitative ones. For example, in the dog bone or ring mold tests one measures either length or width of cracks and a qualitative index is thus obtained [4]. What is more useful, and can be an enabling tool, is a measure of the stresses and strains that develop during solidification. More importantly, knowledge of the rate of strain development during solidification will shed much light on the development of hot tears during casting. Furthermore, a repeatable test is a prerequisite that can be standardized and utilized by the industry. This has been the driving vision of the hot tearing work at ACRC. With this goal in mind, WPI and CANMET MTL (both members of the Light Metal Alliance) joined forces and developed a quantitative method to evaluate hot tearing during solidification. A constrained rod method was used, and contraction force, displacement and temperature change were measured [5].

Li evaluated hot tearing characteristics of alloys A356 and M206 using the constrained rod mold – see Table 1 [6]. Li found that A356 has a higher resistance to hot tearing than M206; this is well known in practice but she was able to quantify the behavior of these

two alloys. In addition, she measured the linear shrinkage of A356 and M206 and showed that M206 has a larger displacement than M356.

Table 1: Chemical Composition of Alloys M206 and A356 (wt.%)

Alloy	Si	Fe	Cu	Mn	Mg	Ti	Al
A206	0.05	0.05	4.55	0.36	0.25	0.006	Bal.
M356	6.7	0.06	<0.01	<0.001	0.38	0.14	Bal.

Since A380.1 and A390 are widely used commercial cast binary Al-Si aluminum alloys, they are studied in this thesis. Because the eutectic point of Al-Si alloys is about 11.7 wt.% silicon [7, 8], A380.1 is Al-Si hypoeutectic [9], whereas A390 is Al-Si hypereutectic [10]. By considering the amount of silicon in the chemical composition of A380.1 and A390, one can examine the differences of the hot tearing tendency quantitatively between these two Al-Si alloys.

Early studies on hot tearing mainly focused on cast aluminum alloys [2]. However, wrought aluminum alloys are also very important in industry. Therefore, the constrained rod method should be applied not only to cast aluminum alloys, but also to wrought aluminum alloys in order to expand the database to establish a new index. To achieve this goal, a second category of alloys was chosen. This group included two wrought aluminum alloys, 6061 and 7075. Alloy 6061 with magnesium and silicon as its major elements is one of the most common aluminum alloys for general purpose use. It has good mechanical properties and exhibits good weldability [11]. Alloy 7075 containing zinc as the primary element is often used in transport applications [12], because it has good strength, average machinability and less resistance to corrosion as compared with other aluminum alloys [13].

In order to broaden the scope of this study, a third category of aluminum alloys was included, the cast aluminum alloy A380.1 with respective additions of strontium and oxides.

Although Al-Si alloy is characterized by high strength, good castability and excellent corrosion resistance, eutectic Si in untreated Al-Si foundry alloys is often very coarse [14]. Since the microstructure of eutectic Si can influence the hot tearing tendency,

modification of eutectic Si is usually a method to improve the hot tearing resistance. This can be accomplished by adding certain chemical modifiers [15].

Strontium is a usual modifying addition used in Al-Si alloys. It has low oxidation sensitivity and the strontium addition as reported can affect the mechanical properties of Al-Si alloys [14]. The reason for this change is that the eutectic silicon facets are absorbed by strontium. Modification by such trace elements can tailor the morphology of silicon crystals from coarse, large platelets to a fine and globular-fibrous microstructure [16, 17]. To illustrate this effect of strontium on an Al-Si alloy, take the example of A357. Figure 1 shows the microstructures of aluminum alloy A357 modified with different weight percentages of Sr.

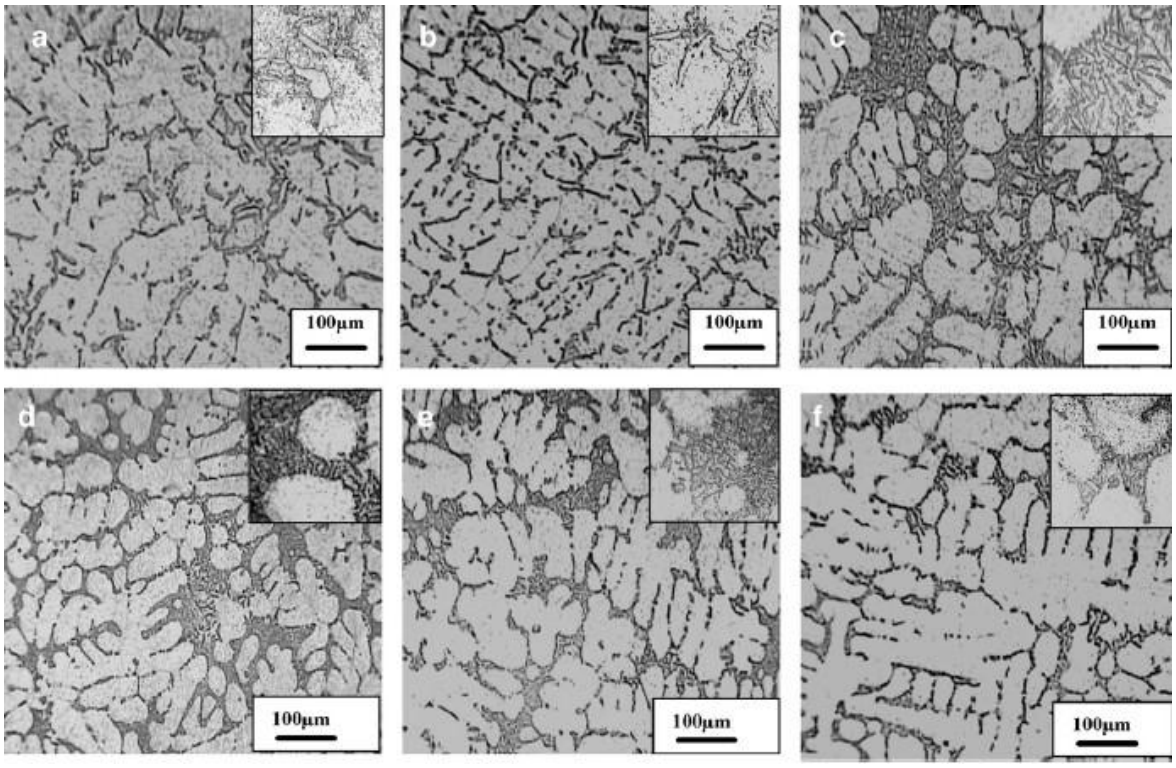

Figure 1: Optical micrograph of A357: (a) non-modified, (b) modified with 0.01%Sr, (c) modified with 0.02%Sr, (d) Modified with 0.03%Sr, (e) modified with 0.05%Sr, and (f) modified with 0.1%Sr [16]

M.M. Haque [18] found that strontium when added to an Al-Si hypoeutectic alloy can modify the microstructure and improve the tensile properties of alloys cast in a metal mold. Because the microstructure has a great impact on the behavior of hot tearing in an

alloy, strontium may also have an impact on an Al-Si alloy's hot tearing resistance. This thesis reports the effect of the addition of strontium into aluminum alloy A380.1 with 0.03wt.% Sr. Then the results of the hot tearing tendency are compared for pure A380.1 and A380.1 modified by the addition of strontium.

Inclusions, which are defined as the impure particles introduced into metal, can influence both the microstructure and the mechanical properties of alloys. The most common inclusion in aluminum alloys is oxide. Oxides can be easily formed in aluminum alloys during the stirring and pouring steps of the casting process [19]. M. Di Sabatino [20] found that oxide inclusion can decrease the fluidity of the melt during casting in Al-7wt.%Si alloy. The more oxides being added, the lower fluidity of the melt will be. Oxide inclusion can also greatly increase the amount of defects, which influence the mechanical properties of aluminum alloys, a consideration that is important to shape forming and the material's behavior during its use [21, 22]. According to Campbell [23], the strength of aluminum alloy castings is greatly weakened by inclusion of oxides within the casting. Previous studies have not focused on quantitative testing for the study of the effect of inclusion on hot tearing in cast aluminum alloys. However, in this experiment, the focus was on quantitative analysis, and A380.1 was chosen as the target to help study the influence of oxides on hot tearing tendency.

2. Objectives

Hot tearing is one of the pivotal issues in casting. It is complicated and influenced by many factors. Previous studies have developed various theories to clarify the mechanism of hot tearing but there has been no consensus. Past conventional hot tearing tests have provided a qualitative index by measuring the cracks on the castings. It is more difficult to set up a quantitative experiment, and such a test is limited as to repeatability. By adopting the new method, the constrained rod method, we can eliminate the problems mentioned above.

The primary objective of this thesis is to use a new simple quantitative and reliable methodology to quantitatively study the hot tearing tendency in both cast aluminum alloys and wrought aluminum alloys.

The second objective is to investigate the hot tearing tendency of cast aluminum alloy in the presence of different additions. Strontium and oxide inclusion were the two additions chosen for this thesis. Since strontium can affect the microstructure in hypoeutectic Al-Si alloys, the experiment involved hypoeutectic binary Al-Si alloy A380.1. By analyzing the difference of the hot tearing tendency between pure A380.1 and A380.1 in the presence of different additions, the effect of strontium or oxide inclusion on hot tearing could be elucidated quantitatively during solidification.

Another objective in the thesis is to establish a new hot tearing index for all the alloys tested on the constrained rod mold. The comparisons of the quantitative data for load, displacement and temperature were made for different alloys, including A380.1, A390, 6061, 7075, and A356, M206 [24].

The constrained rod mold data proved to be valuable in ultimately establishing a new quantitative method. At the same time, examinations of the microstructure and crack morphology of alloys helped determine the hot tearing tendency.

3. Background and literature review

According to Li's paper [5], the Instrumented Constrained Rod Mold was designed to simultaneously measure two kinds of data: (1) the load, time and temperature developed during solidification for a restrained casting can be acquired with a load cell; (2) the contraction (displacement), time and temperature for a relaxed casting are available with a linear variable differential transformer (LVDT). The temperatures and load/displacement data can be recorded by a PC-based National Instrument data acquisition system. The system consists of SCXI-1303 terminal block, PCI-6043E interface card and LabVIEW software (DASYLab). Figure 2 shows the diagram of the instrumental set-up.

The testing piece is composed of two arms and a riser at the center. A slight taper of the arm reduces friction between the mold and the casting during solidification. The right arm (Figure 2) is constrained at the end with a steel bolt embedded in the casting and a graphite holder anchoring the bolt tightly. The left arm (Figure 2) is used for temperature and load/displacement measurements. Its end is connected to a load cell (Loadstar iLoad Pro Analog 500lb.) or LVDT (Macro Sensors HSTA 750-1000). The LVDT can move freely in a horizontal direction, while the load cell will offer resistance to the contraction. The mold is closed via a hydraulic system under constant pressure for each test, and heat plates control the mold temperature.

Figure 3 is a schematic illustration showing the components of the apparatus. In the diagram of casting dimensions (Figure 4), two K-type thermocouples are used for temperature measurement; one is positioned at the riser end (T1) where hot tears are expected to occur, and the other one at the end of the rod (T2). Figure 5 shows the load cell and LVDT setup and the positions for the K-type thermocouples, and Figure 6 provides an overview of the experimental setup, including an induction furnace, the Instrumented Constrained Rod Mold, and the PC-based National Instrument data acquisition system.

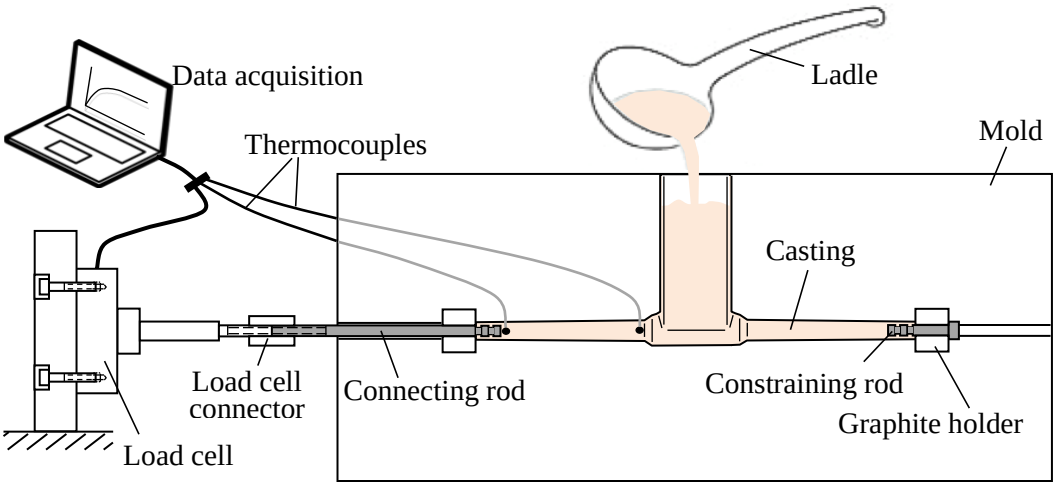

Figure 2: Diagram of experimental set-up

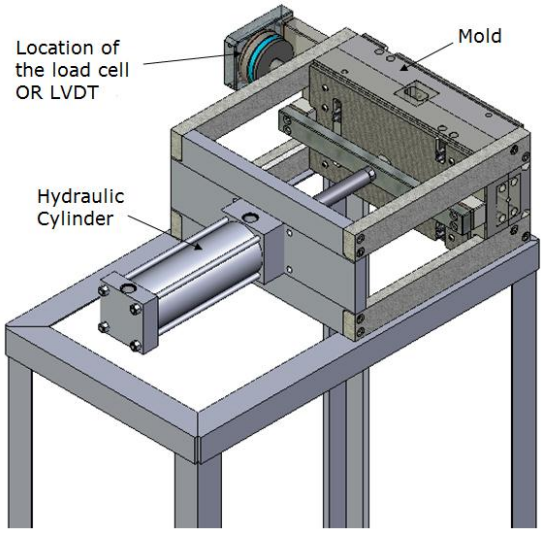

Figure 3: Mold assembly

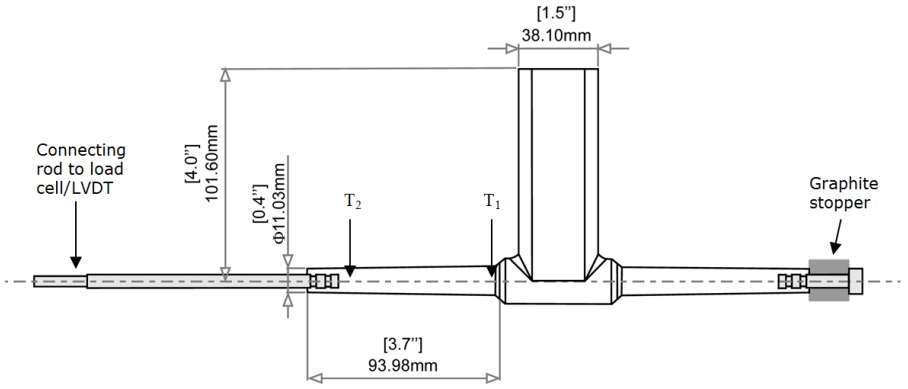

Figure 4: Casting dimensions

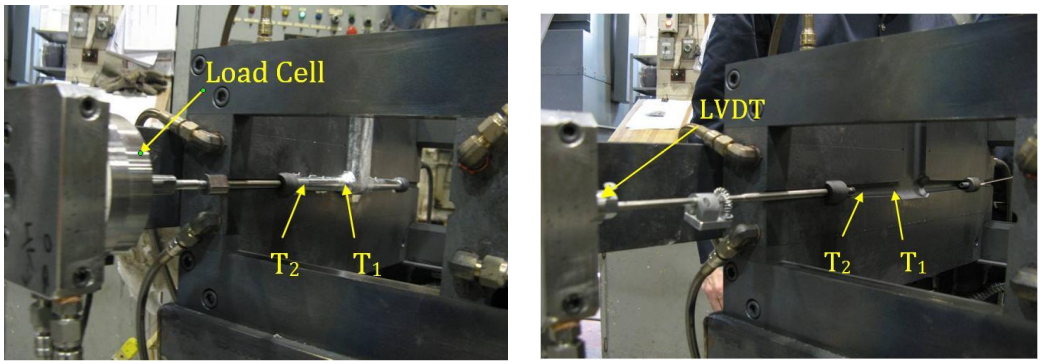

Figure 5: Load cell and LVDT setup

Figure 6: Experimental setup

When analyzing the data acquired by the Instrumented Constrained Rod Mold, one can pinpoint the onset of hot tearing and learn the tensile coherency from three types of data, the load curve, its first derivative and the temperature curve. Hot tearing's propagation can also be detected from the derivative of the load curve. One can also acquire the linear displacement/contraction during the solidification for different alloys by using the LVDT. Since hot tearing is alloy-dependent, it becomes convenient to compare the load, displacement and temperature curves of various alloys and investigate repeatedly their hot tearing tendency by this quantitative method.

Using this method, Li [24] studied the effects of mold and pouring temperatures on hot tearing of two cast aluminum alloys, A356 and M206. Li selected three different mold temperatures, 200˚C, 300˚C and 370˚C, for the experiment. The results of load, temperature and displacement are shown in the following figures (Figures 7 and 8). At a

lower mold temperature (200 ˚C) (Figures 7a and 8a), the load started developing (load onset) faster than at a higher mold temperature. As shown in the first derivative curves (Figures 7b and 8b), it is worthwhile noting that hot tears propagated more slowly at higher mold temperature for both alloys. No hot tearing forms at three different mold temperatures for A356, while M206 shows significant hot tearing preference under the same casting conditions.

Li studied the effects of three additional pouring temperatures, 700 ˚C, 750˚C and 800˚C, on M206 (Figure 9). The propagation of hot tearing was more gradual at the lowest pouring temperature. For the highest pouring temperature, the load suddenly released. Once the loading rate hit zero, it indicated the casting bar broke at that moment. Li offers two possible reasons to explain why the severity of hot tearing increased with a higher pouring temperature: (1) a lower cooling rate increases the grain size, thereby decreasing the ability of the structure to accommodate the accumulating stress; (2) the increment in liquid film thickness between grains tends to increase the hot tearing tendency.

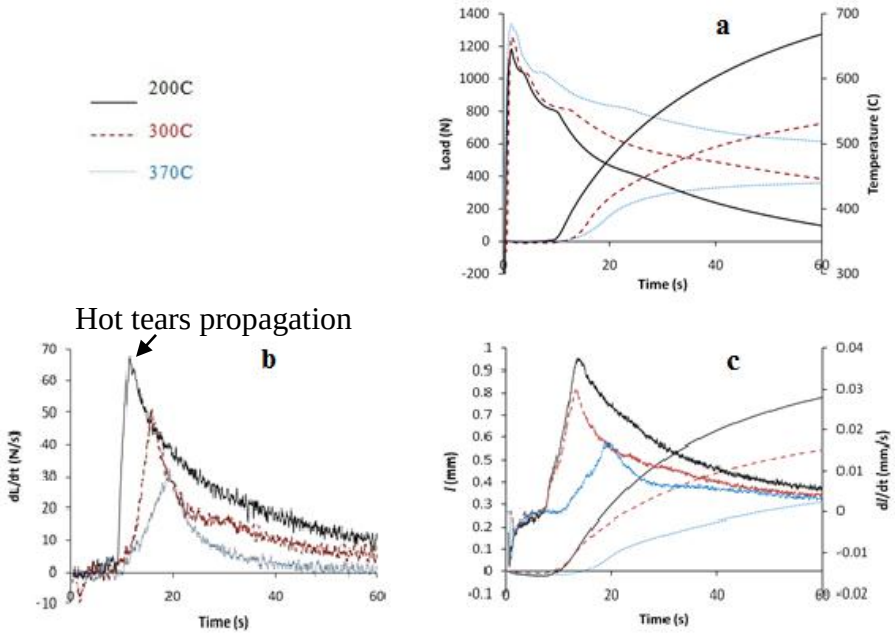

Figure 7: (a) Temperature and load development as a function of time for A356 at different mold temperatures, temperature measured at centerline of the rod at the riser end (Tc1); (b) Derivative of load vs. time curves; (c) Measured displacement and its derivative as a function of time

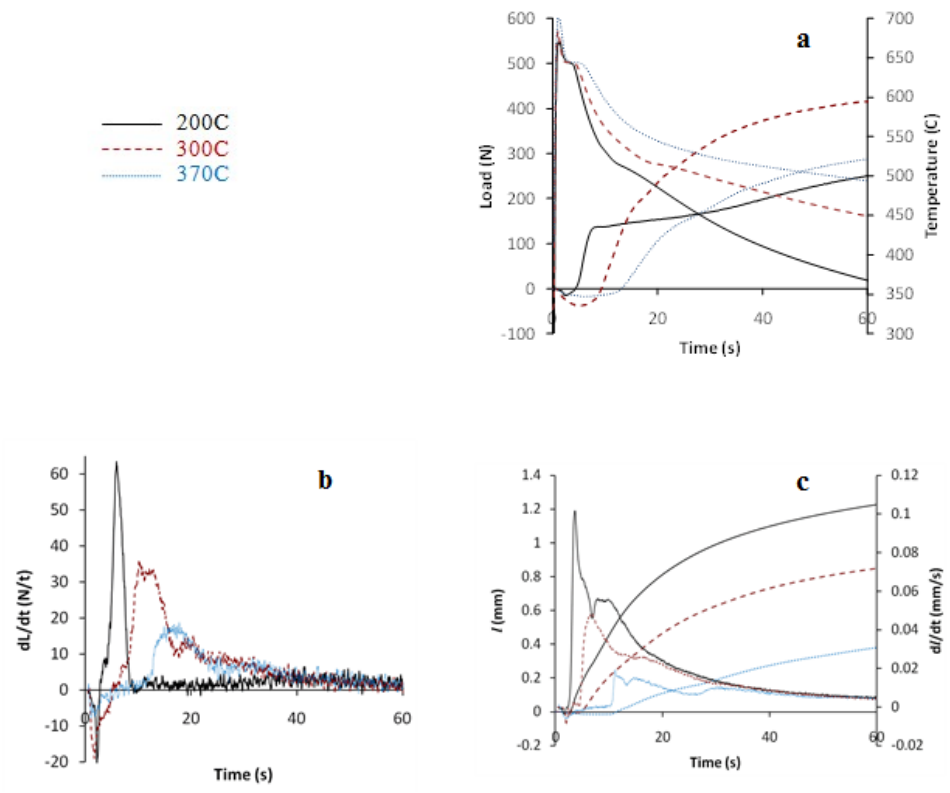

Figure 8: (a) Temperature and load development as a function of time for M206 at different mold temperatures, temperature measured at centerline of the rod at the riser end (Tc1); (b) Derivative of load vs. time curves; (c) Measured displacement and its derivative as a function of time

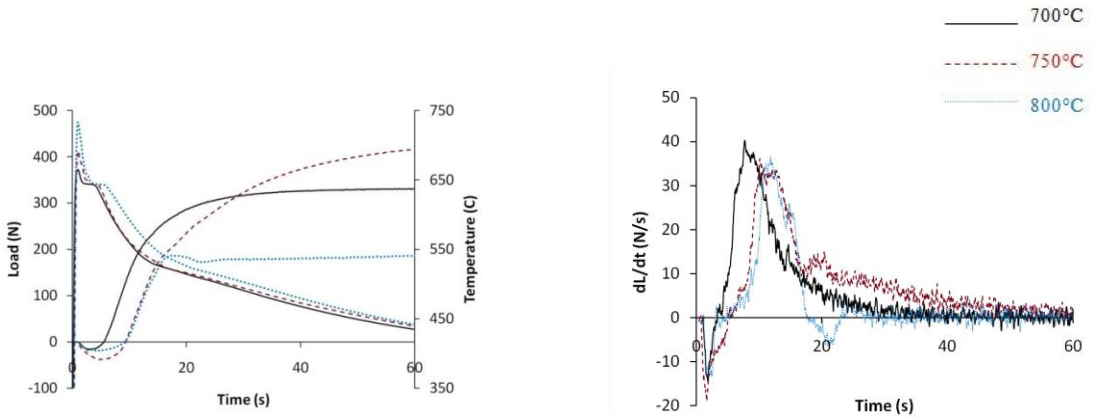

Figure 9: Left diagram: Temperature and load development as a function of time for M206 at different pouring temperatures, temperature measured at centerline of the rod at the riser end; Right diagram: Derivative of load vs. time curves

The significance of Li's work is its reliability, so it becomes possible for one to evaluate hot tearing in a quantitative manner. Previous work conducted by Li established the foundation and set the benchmark for the current research in this thesis on four additional aluminum alloys. Since Li pointed out that the mold and pouring temperatures can exert significant influence on hot tearing, appropriate mold and pouring temperatures were carefully chosen at the outset of this research.

Li [24] also investigated the effects of grain refiner on M206 by using the Instrumented Constrained Rod Mold. Al-Ti and Al-Ti-B master alloys were added to the melt as the grain refiner to achieve fine equiaxed aluminum grains [25]. In addition to superior mechanical properties, fine equiaxed grain structures are expected to produce uniform distribution of secondary phases and micro-porosity in castings, thereby resulting in good surface finish, high tolerance to hot tearing and machinability [26]. The effects of grain refinement on load onset in Li's work were complex, because they are related to both grain size and morphology of the casting, which affect the refilling of incipient cracks at an early stage.

Besides Li's experiments with grain refiner, no other work has been done to check the effects of other additions on hot tearing by using this new method. In this thesis, the strontium and oxide inclusion were separately added into the cast aluminum alloy A380.1 and tested on the Instrumented Constrained Rod Mold.

4. Experimental procedure

The experimental section is divided into 3 parts: (1) alloys, (2) apparatus and operational procedures, and (3) hot tearing index.

4.1 Alloys

In order to enrich the database for the new method, this thesis tested two commercial cast binary Al-Si aluminum alloys A380.1 and A390 and two wrought aluminum alloys 6061 and 7075. Of the cast aluminum alloys, A380.1 is Al-Si hypoeutectic, while A390 is Al-Si hypereutectic. In the wrought aluminum alloys, magnesium and silicon are the major elements of alloy 6061, while zinc is the primary element of alloy 7075. In addition, a 0.03wt.% strontium and an oxide inclusion were added into alloy A380.1 respectively to study their effects on hot tearing. Chemical compositions of alloys were measured by a spark emission spectrometer. Table 2 shows the melting ranges of these alloys.

Table 2: Melting ranges of alloys

Alloy	A380.1	A390	6061	7075
^{o}F	1000-1100	950-1200	1080-1205	890-1175
^{o}C	540-595	510-650	582-652	477-635

4.2 Apparatus and operational procedures

Melting was conducted in an induction furnace, and the Instrumented Constrained Rod Mold was used to acquire the quantitative data of load, displacement and temperature for different aluminum alloys. The mold was prepared during the melting, which involved the installation of the load cell or LVDT. The rod and steel bolt were inserted with graphite holders, and the connection between the rod and the load cell/LVDT was also completed. Then the mold was closed via the hydraulic system and heated up to 200^{o}C before pouring. According to Li's paper [24], the temperature measurement would interfere with other measurements when the temperatures and load or temperatures and displacement were measured in tandem. The reason Li gives for this is that the thermocouples placed inside the casting add a resistance to the casting contraction. For this reason, the temperature was measured separately in parallel tests.

The pouring temperature for all alloys was set at 100 ℃ above their individual liquidus temperatures (Table 3). According to the casting dimensions (Figure 4), two temperatures

can be measured in the center of the casting during solidification. However, in this thesis only T1 was measured for calculating the cooling rate. Immediately before pouring, the data acquisition system started to record load and temperature or displacement and temperature simultaneously. After pouring, the castings were extracted from the mold to examine cracks. The test for each alloy was repeated 5-10 times.

Table 3: Pouring temperatures of alloys

Alloy	A380.1	A390	6061	7075
Pouring Temperature (^{o}C)	~700	~750	~750	~735

In the experiments that involved adding strontium or oxide inclusion into cast aluminum alloy A380.1, 10wt.%Sr strontium-aluminum alloy provided the additional strontium, while small pieces of potatoes were added into the melt to introduce oxides. In order to fully dissolve the respective addition, the melt was kept at about 700^{o}C for 40 minutes. The compositions of all the alloys were measured using a spark emission spectrometer.

During each experiment, one test casting was selected for hot tearing measurement and microstructure analysis. The samples were placed at the locations shown in Figure 10. Sample #1 was taken from the left arm, which was connected to the load cell. The arm was sectioned longitudinally along its centerline and the longitudinal cross sections were analyzed. Sample #2 was taken from the right arm, and its transversal cross section was used for the microstructure examination.

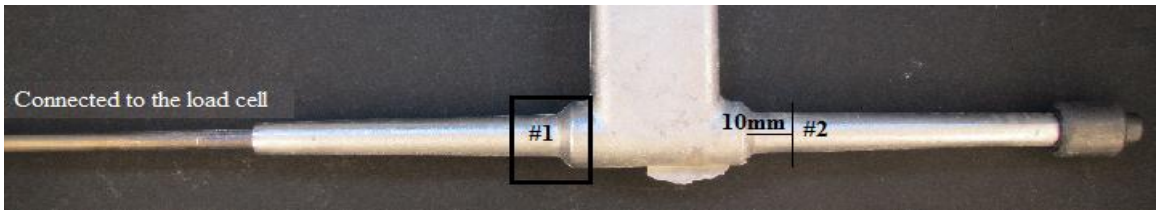

Figure 10: The positions of samples for microstructure analysis

All the samples were cold mounted in epoxy, followed by grinding and polishing procedures, and being etched with 5vol.% HF solution. Then, the microstructures were analyzed by optical microscopy and a scanning electron microscope (SEM). The total area of cracks in the center longitudinal cross sections (hot spot) was measured using the software ImageJ. In the case of A380.1 containing the oxide inclusion, the Energy Dispersive Xray (EDX) was used to determine the existence of oxides.

4.3 Hot tearing index

Li listed two criteria for judging the hot tearing tendency, which are also used in this research: (1) the total area of cracks in the center longitudinal cross sections calculated by ImageJ is used as a reference for the hot tearing index; (2) the curves of the temperature, load, and the first derivative of load against time were plotted (Figure 11 [6]). From these curves of load and its first derivative, one can identify the load onset, crack initiation and propagation and relate them to time quantitatively. Solidification data of alloys, including their liquidus, solidus and cooling rate can also be obtained from the temperature vs. time curve. Correlations between measured data, alloy solidification characteristics and hot tearing formation can be established quantitatively by combining and comparing these curves.

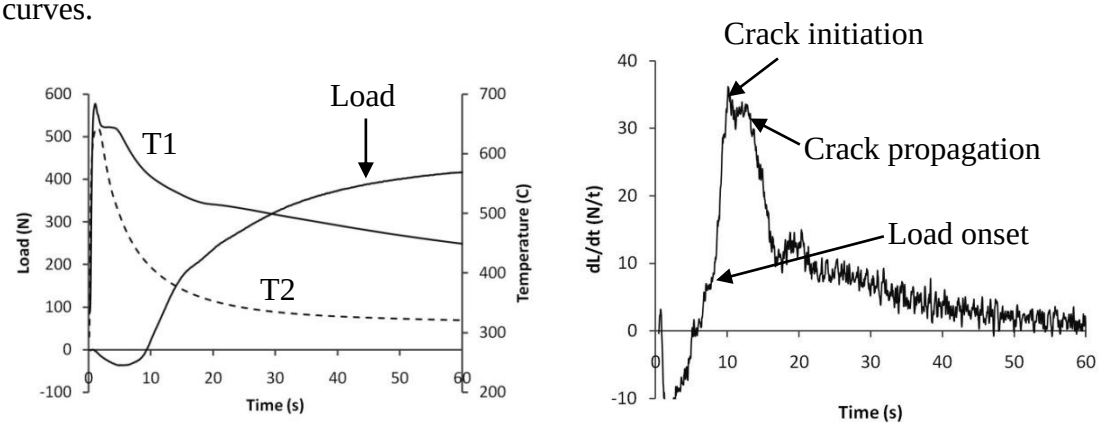

Figure 11: (a) Temperatures and load development as a function of time for M206; (b) Derivative of load vs. time curves

In addition to the above two criteria, this thesis used a third criterion. A new hot tearing index was established based on the derivative curves of load for different aluminum alloys. For alloys without cracks after solidification, calculating the incipient crack loading rate helps identify the hot tearing tendency. For alloys with large cracks, the speed of the change in the loading rate provided the hot tearing index. By combining the information from the no-crack and large-crack studies, and after normalization, a new hot tearing tendency was established based on the quantitative results acquired from the Instrumented Constrained Rod Mold.

5. Results and discussion

This section presents and analyzes the results of tests performed on four groups of alloys: (1) cast aluminum alloys A380.1 vs. A390; (2) wrought aluminum alloys 6061 vs. 7075; (3) A380.1 vs. A380.1 modified with strontium; and (4) A380.1 vs. A380.1 with added oxides.

There are several considerations in analyzing these alloys: (1) the chemical compositions of the alloys; (2) the profile of load/displacement/temperature vs. time during the solidification; (3) microstructures, crack images, and fractographs.

Since very consistent results are obtained after repeated experiments for each alloy, one casting from each sample was chosen for analysis in this thesis. For all the alloys, the starting point of solidification was normalized as the melt entry, which was determined by the thermocouple at T1. Load is the tensile force during casting due to solidification shrinkage and thermal contraction, while the displacement is caused by the linear contraction of the rod. During the experiment, slight decreases of the data are usually observed at the beginning of load and displacement for alloys, which is caused by the melt pressure occurring at the initial contact with the connecting constraining rod after the pouring. At the same time, by calculating and plotting the first derivatives of both load and displacement, the load and displacement rate can be obtained. The incipient crack loading rates for different alloys were also listed. When the incipient crack was immediately refilled through mass feeding, the load rate would change due to this procedure. Then, after the refilling, the load continued to increase. Temperature (T1) here represents the cooling curve for each alloy.

Finally, these experiments contributed to formulating a new hot tearing index, which includes the results from Li's studies [24] on A356 and M206.

5.1 Cast aluminum alloys

Table 4 gives the chemical compositions of cast aluminum alloy A380.1 and A390. Note that the sample of A390 reveals a higher fraction of Si than A380.1.

Table 4: Chemical compositions of alloys A380.1 and A390 (wt.%)

Cast Alloy	Si	Fe	Cu	Mn	Mg	Ti	Ni	Zn	Sn	Al
A380.1	8.26	0.7	3.77	0.1	0.06	0.02	0.054	1.54	0.024	Bal.
A390	16.8	0.87	4.5	0.13	0.6	0.07	0.05	1.13	-	Bal.

5.1.1 Load, displacement and temperature measurements

The load, temperature and displacement data recorded during the solidification of A380.1 and A390 are shown in Figure 12. For alloy A380.1, at around 4.6 seconds, the contraction started and developed rapidly during solidification. The maximum loading rate reached 80N/s, and the total load within 60 seconds was 1400N. The linear displacement at 60 seconds was 1.09mm for the effective 75mm length of the rod, and its maximum rate was 0.052mm/s. For the A390 alloy, the contraction began at 8.5 seconds and increased slowly. Before the load onset, there was a slight decrease in load, which was caused by the pressure of the melt just after the pouring. With a small loading rate of 21N/s, load reached only 879N after 60 seconds. The total linear displacement of A390 at 60 seconds was 0.59mm, which is much smaller than that of A380.1. The maximum displacement rate of A390 was also smaller than that of A380.1. This phenomenon may be associated with the different silicon percentage in the two alloys. Since silicon has a larger density in a liquid state than in a solid state, it does not contract when it freezes. As A390 contained more silicon than A380.1, A390 contracted less than A380.1.

According to Table 5, the incipient crack loading rate of A380.1 was 15, and the incipient crack loading rate of A390 was 10. There were no cracks found because the incipient cracks filled by liquid were in the early stage of solidification. Since A380.1 has a larger incipient crack loading rate than A390, it has a stronger hot tearing tendency than A390.

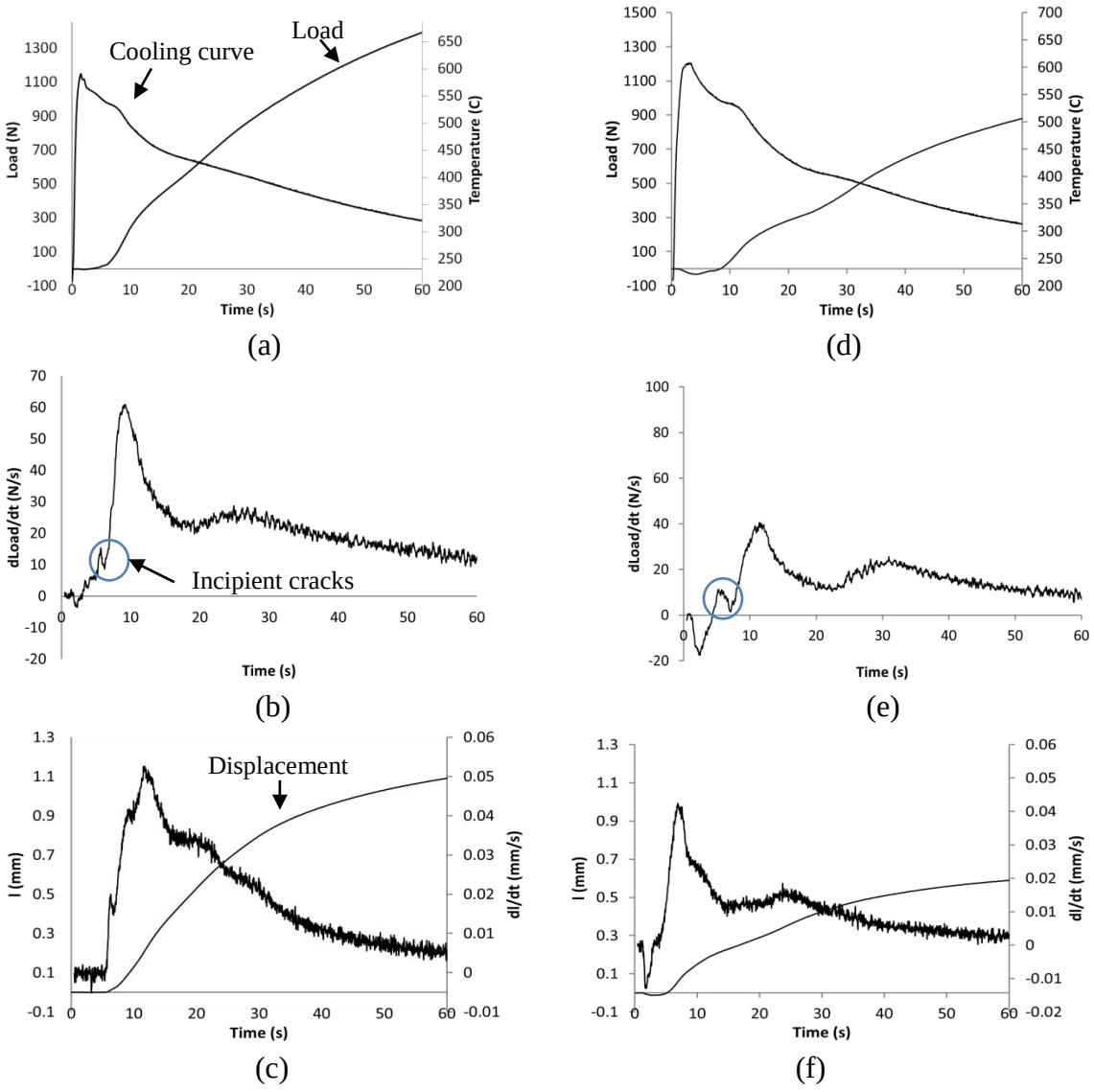

Figure 12: (a) Load development and temperatures vs. time for A380.1; (b) Derivative of load vs. time curve for A380.1; (c) Displacement and its derivative vs. time for A380.1. (d) Load development and temperatures vs. time for A390; (e) Derivative of load vs. time curve for A390; (f) Displacement and its derivative vs. time for A390

Table 5: Contraction force and linear displacement measurement data

Alloy	Incipient crack loading rate (N/s)	Maximum loading rate (N/s)	Load @ 60 seconds (N)	Maximum displacement rate (mm/s)	Displacement @ 60 seconds (mm)
A380.1	15	62	1400	0.052	1.09
A390	10	41	879	0.042	0.59

5.1.2 Mosaic optical micrograph and microstructure

No obvious hot tears were found on the surface after solidification. Once sample #1 was taken out from the casting, there were still no hot tears found for both alloys A380.1 and A390 in the longitudinal cross section of the neck region, the critical region (Figure 13).

In the eutectic Al-Si alloy, the Si composition is about 11.7wt.% [7]. In the case of alloy hypereutectic A390 with 16.8wt.% Si, primary Si forms first. Compared to the microstructure of A380.1 (Figure 14), the primary Si produces a large diamond phase which can be seen in the micrograph of A390 (Figure 15). The eutectic mixture is non-lamellar in form and appears to consist of separate flakes.

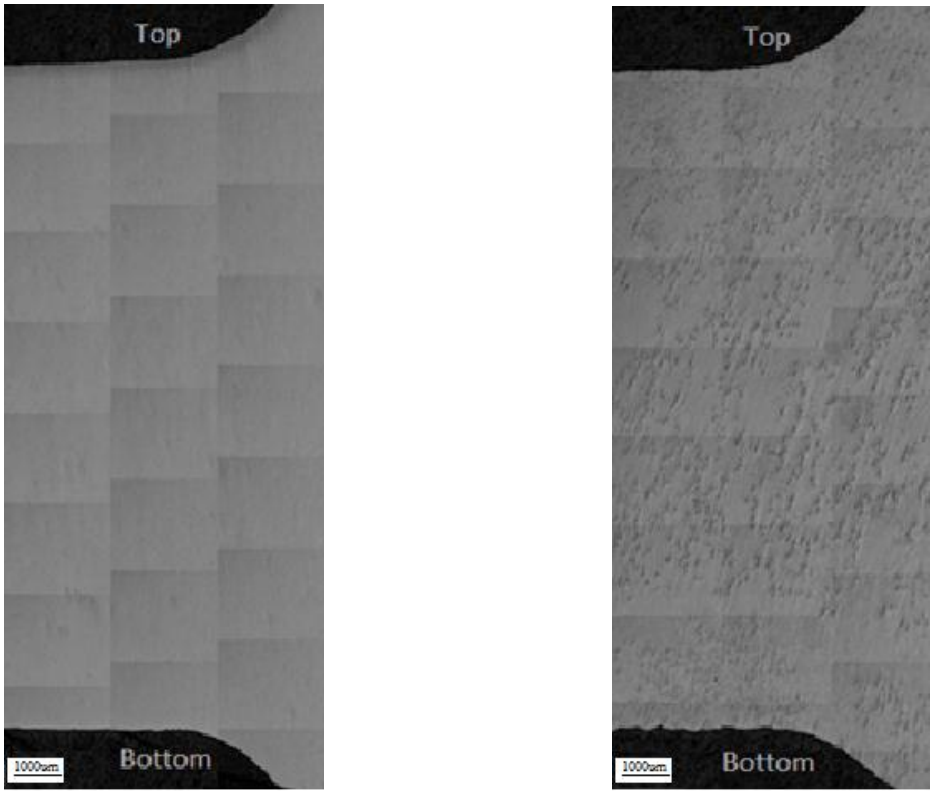

(a) (b)

Figure 13: (a) Mosaic optical micrograph showing the longitudinal cross section of the neck region of A380.1; (b) Mosaic micrograph in the neck region of alloy A390

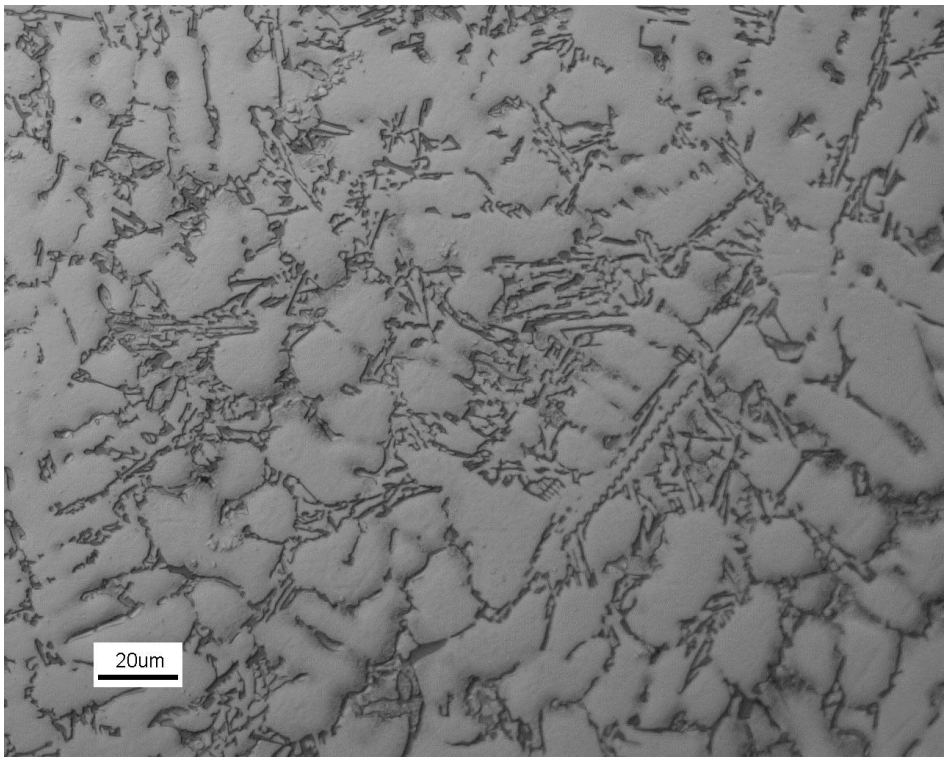

Figure 14: Optical micrograph of A380.1

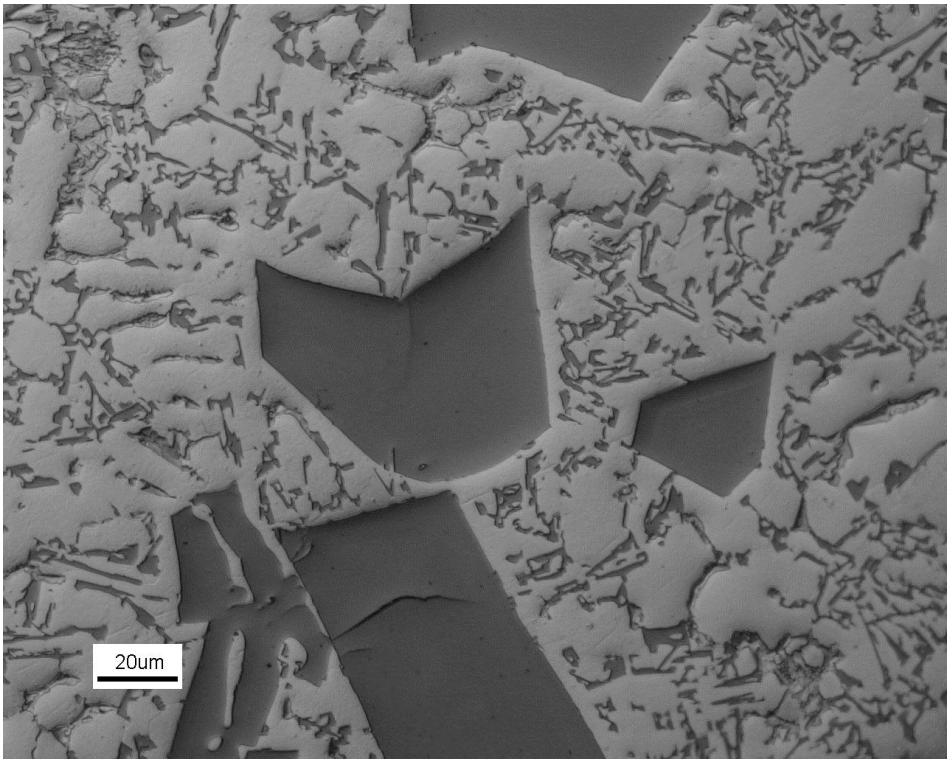

Figure 15: Optical micrograph of 390

5.2 Wrought aluminum alloys

The chemical compositions of wrought aluminum alloys 6061 and 7075 are given in Table 6. Major elements of alloy 6061 are magnesium (1.2wt.%) and silicon (0.62wt.%). Alloy 7075 contains 5.6wt.% zinc.

Table 6: Chemical composition of wrought alloys 6061 and 7075 (wt.%)

Wrought Alloy	Si	Fe	Cu	Mn	Mg	Cr	Zn	Ti	Al
6061	0.62	0.08	0.35	0.02	1.2	0.14	0.002	0.002	Bal.
7075	0.39	0.67	1.85	0.05	5.0	0.26	5.6	0.02	Bal.

5.2.1 Load, displacement and temperature measurements

The load, temperature and displacement data recorded during the solidification of wrought aluminum alloys 6061 and 7075 are presented in Figure 16 and Table 7. For alloy 6061, during solidification, the contraction started and developed quickly at around 5.7 seconds. The increase of load was interrupted at 6.5 seconds. An abrupt drop represented the release of load corresponding to the occurrence of hot tear. The maximum loading rate for the increase was 74N/s, and for the decrease was -20N/s. The total linear displacement at 60 seconds was 0.86mm for the effective 75mm length of the rod, and its maximum displacement rate was 0.069mm/s. At 60 seconds, the load merely reached 150N. For alloy 7075, the contraction began at 5.1 seconds and increased with a maximum loading rate of 72N/s. After the initiation of tear, there was a slight increase in the load rate at 10 seconds. This indicates that tearing may be hindered and some of the cracking is filled by the remaining liquid at the early stage during solidification. Then, the load rate rapidly decreased from 65N/s to 29N/s. At 60 seconds, the load reached 1038N, and the total linear displacement of 7075 was 0.8mm.

In the wrought alloys, it is hard to determine the incipient crack rate on the derivative of load. This may be due to the poor fluidity of wrought alloys, which means it was hard for the remaining liquid to move and fill the incipient cracks. Without enough feeding, hot tears propagated to the final cracks on the casts. In the LVDT data, for wrought aluminum alloys, there was a large "V" shape at its derivative. A possible explanation for this is the rate of displacement was influenced by the development of cracks during solidification. When there was an expansion of the hot tear, the rate of displacement

would decrease until the effect of contraction became large enough to overcome the influence of the hot tear and made the rate of displacement increase again. Because 6061's abrupt change of load rate during solidification corresponded to the absolute rupture, alloy 6061 has a higher hot tearing tendency than alloy 7075.

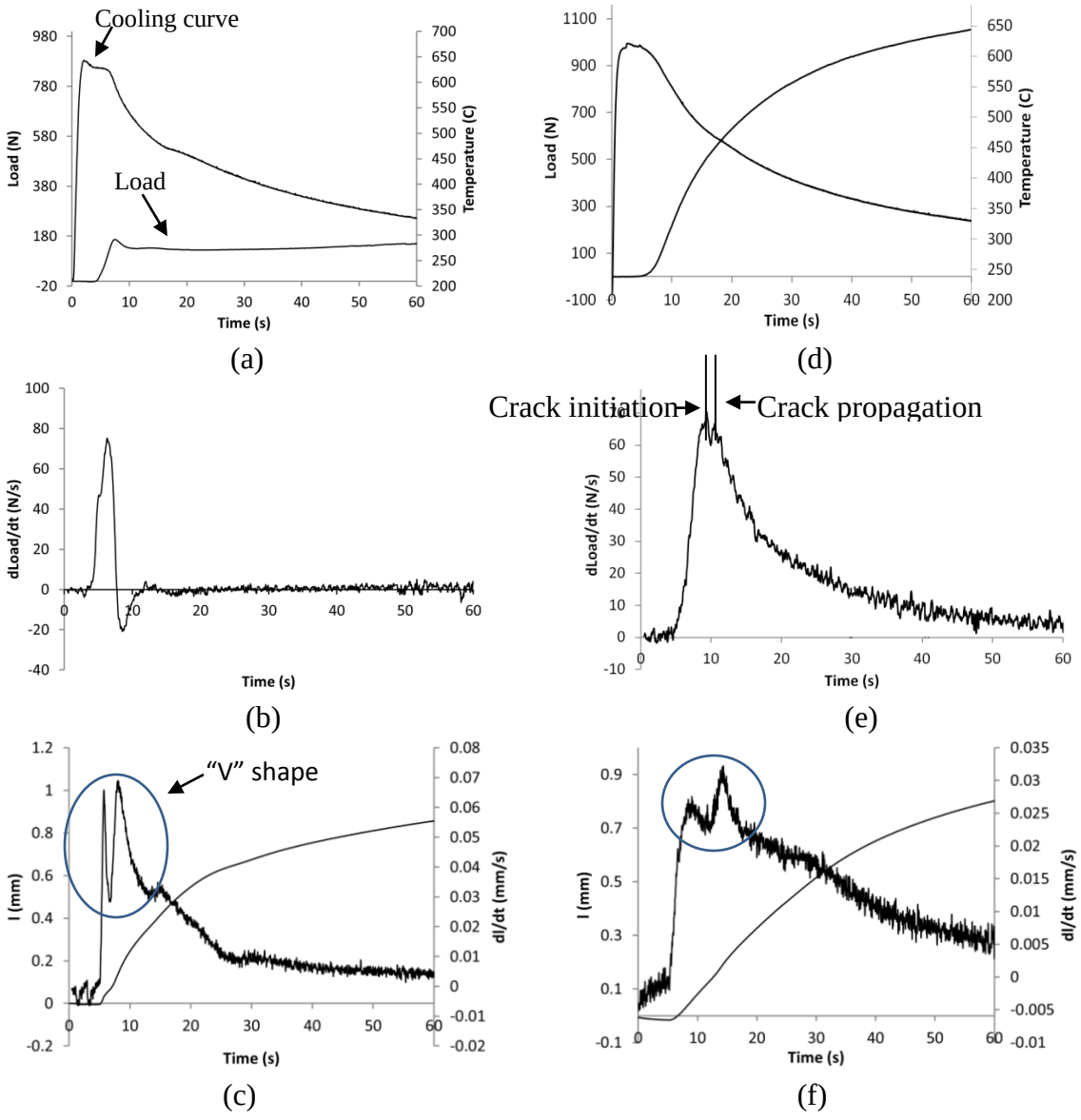

Figure 16: (a) Load development and temperatures vs. time for 6061; (b) Derivative of load vs. time curve for 6061; (c) Displacement and its derivative vs. time for 6061; (d) Load development and temperatures vs. time for 7075; (e) Derivative of load vs. time curve for 7075; (f) Displacement and its derivative vs. time for 7075

Table 7: Contraction force and linear displacement measurement data

Alloy	Maximum loading rate (N/s)	Load @ 60 seconds (N)	Maximum displacement rate (mm/s)	Displacement @ 60 seconds (mm)
6061	+74,-20	150	0.069	0.86
7075	72	1038	0.032	0.8

5.2.2 Metallography of hot tears

In Figures 17 and 18, micrographs show the hot tears for 6061 and 7075. The wrought aluminum alloys have a high susceptibility to hot tearing, and the castings were totally destroyed by big cracks. Both external and internal cracks were detected in alloy 6061 and 7075, and many minor cracks were found around the major cracks. When being taken out of the mold, alloy 6061 was totally broken, with the crack area for 6061 calculated at about 13.6 mm^2. For 7075, around one-third of the total transversal cross-section area was still connected just after the solidification. However, when attempting to get the 7075 sample out of the mold, it broke during the procedure and revealed a crack area of about 9.3 mm^2. Thus, on the basis of the above analysis, 6061 may have a higher hot tearing tendency than 7075.

(a) 6061

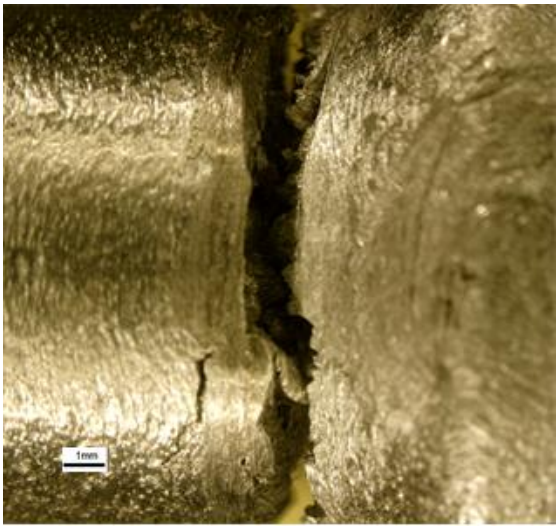

(b) 7075

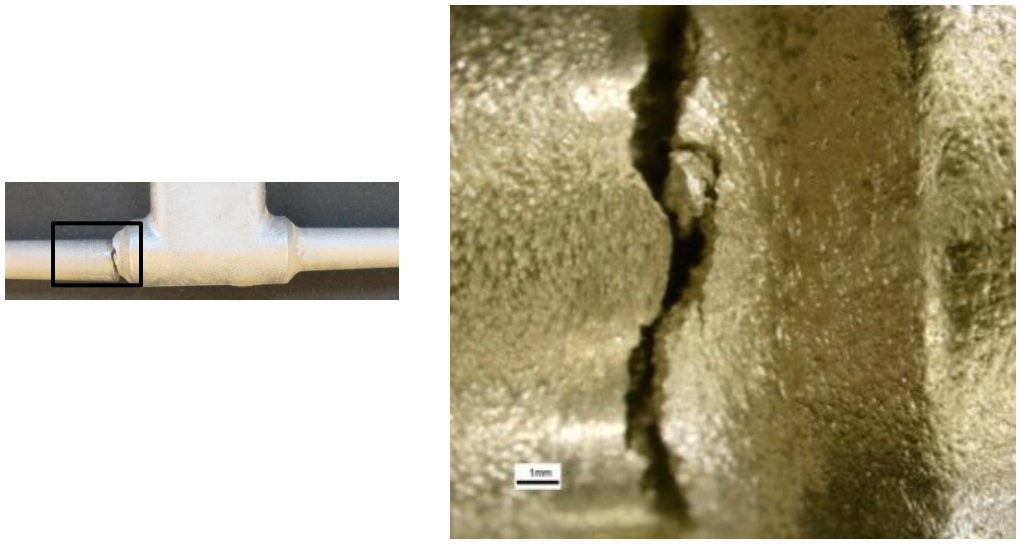

Figure 17: (a) Photographs of the constrained casting showing cracking locations of 6061; (b) Photographs of the constrained casting showing cracking locations of 7075

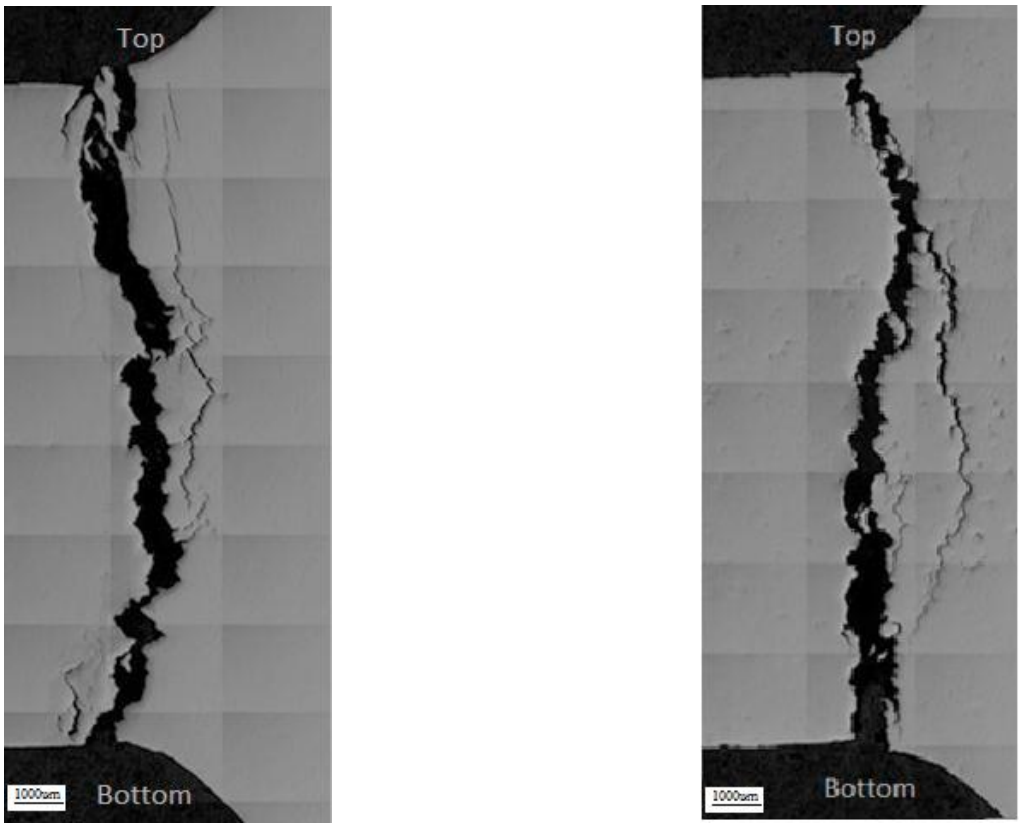

(a) (b)

Figure 18: (a) Mosaic optical micrograph showing the longitudinal cross section of the neck region of 6061; (b) Mosaic micrograph showing hot tears in the neck region of 7075

Fracture morphologies of the hot tearing surfaces of wrought aluminum alloys 6061 and 7075 were studied using SEM. At low magnification (Figure 19), the fractograph of 6061 shows big long dendrites with a clear directional property. The volume contraction of these big grains may lead to hot tears in 6061. For 7075, the hot tearing surface was covered by interdendritic liquid in a few areas; the second phase also formed on this surface. Figure 20 reveals that there was a large brittle fracture region on the hot tearing surface of alloy 7075. This was probably due to removing the cast from the mold instead of to hot tearing. For 6061, the brittle fracture area shrank dramatically. At high magnification (Figure 21), more stretched tiny slices on 7075's hot tearing surface become visible. These slices would be mainly due to the remaining liquid attempting to fill the incipient cracks. Although the filling was never completed, these slices represented the lower hot tearing tendency of 7075 than that of 6061.

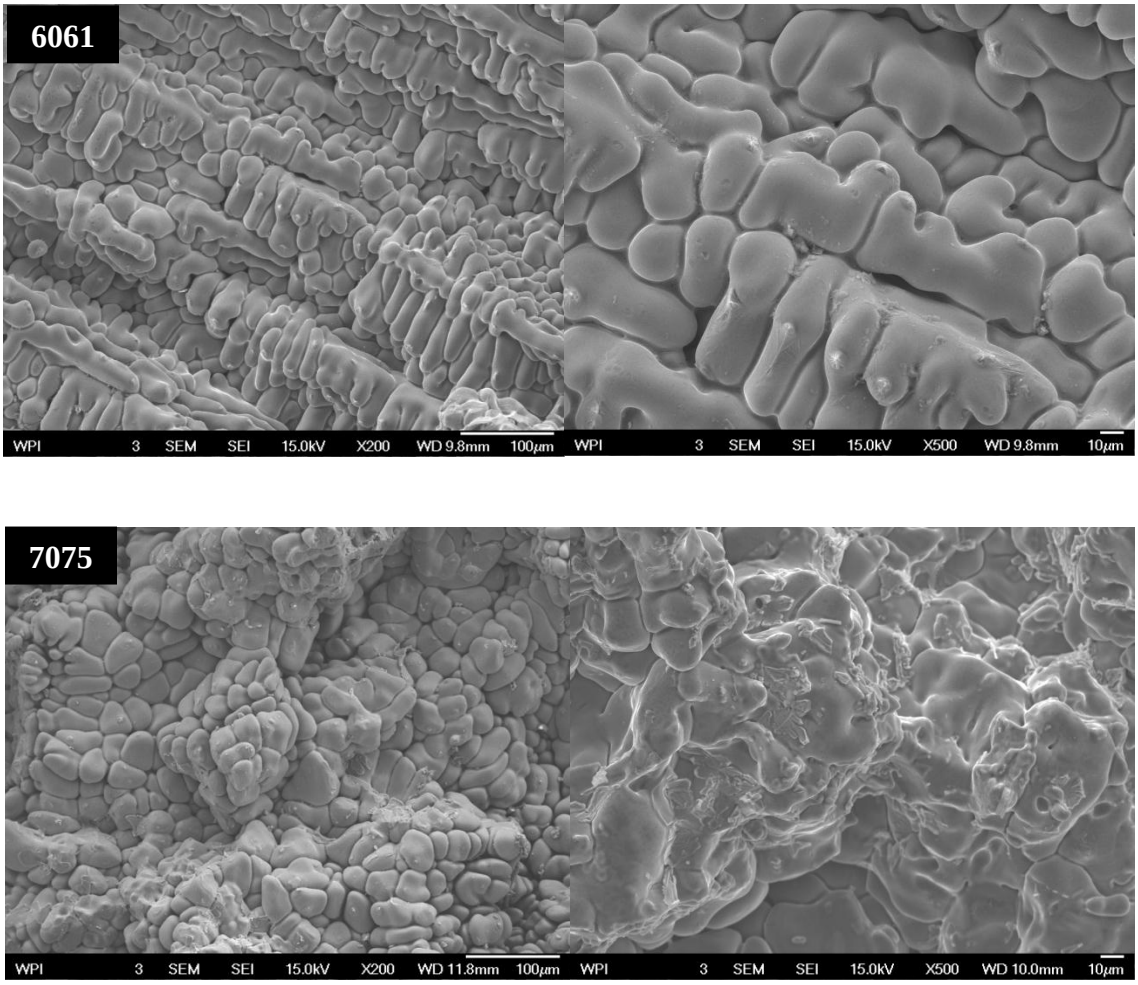

Figure 19: The fracture SEM images of 6061 and 7075 at low magnification

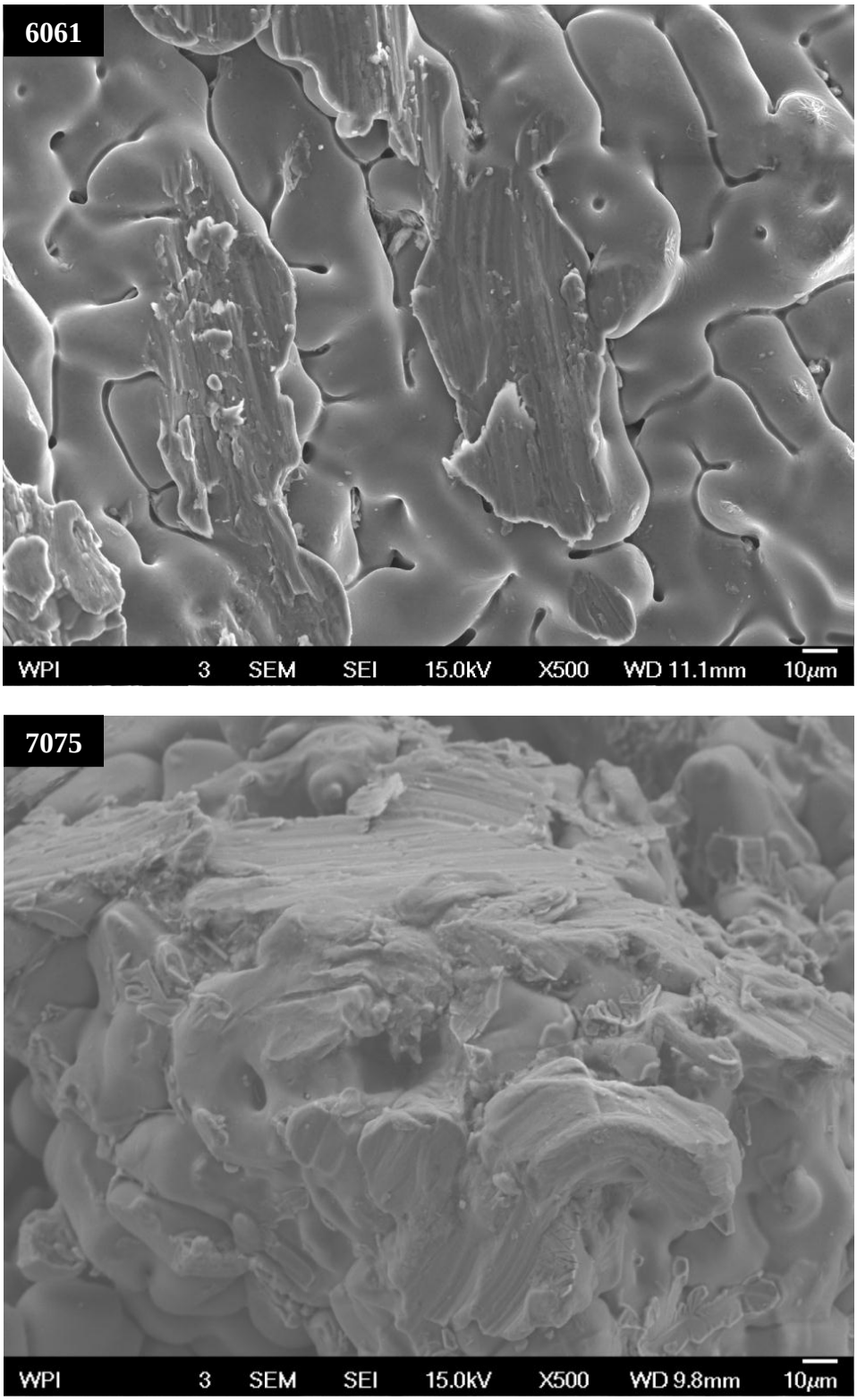

Figure 20: The brittle fracture SEM images of 6061 and 7075 at low magnification

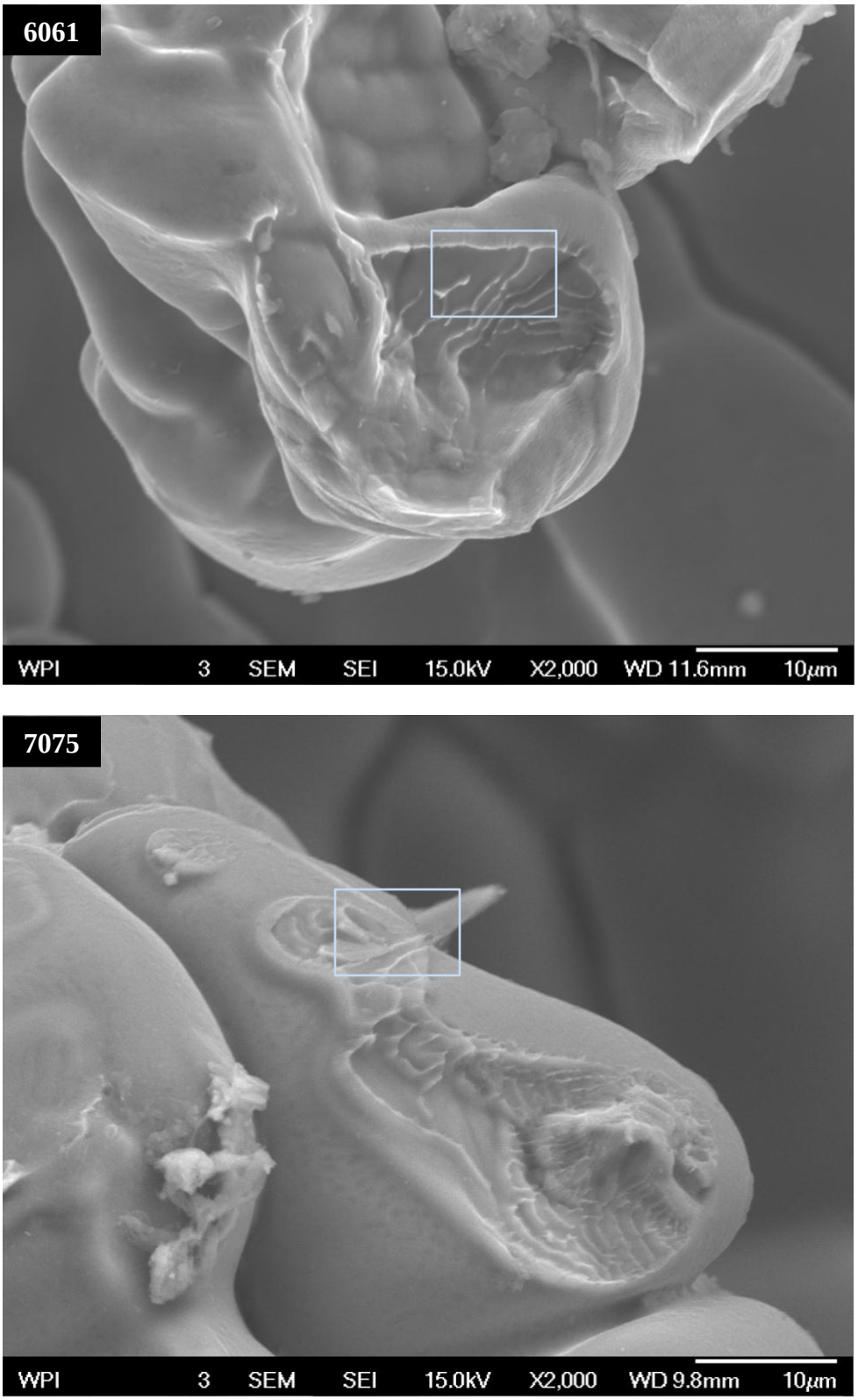

Figure 21: The fracture SEM image of 6061 and 7075 at high magnification

5.3 Effect of strontium

The chemical compositions of A380.1 and A380.1 modified with 0.03wt.% Sr are given in Table 8. Note that the measurement was partly dependent on the position of the sampling point; the resulting data here may thus have some errors compared with real values.

Table 8: Chemical composition of alloys A380.1 and A380.1 modified with Sr (wt.%)

Alloy	Si	Fe	Cu	Mn	Mg	Ti	Ni	Zn	Sn	Sr
A380.1	8.26	0.7	3.77	0.1	0.058	0.02	0.054	1.54	0.02	-
A380.1+Sr	8.29	0.66	3.92	0.1	0.054	0.02	0.051	1.48	0.02	0.03

5.3.1 Load, displacement and temperature measurements

The load, temperature and displacement data recorded during the solidification of A380.1 modified with strontium are shown in Figure 22 and Table 9. At 4.85 seconds, the load of the modified alloy started and increased more rapidly than was the case for pure A380.1 with a 76N/s maximum loading rate for modified A380.1. There was a larger convex on the load curve from 10-20 seconds compared with that of pure A380.1's load curve (Figure 22(a) vs. Figure 12(a)). The LVDT data also validated this phenomenon. In order to figure out the reason, the measurements were integrated with the cooling curve. The temperature at which the large convex occurred was at approximately 570^{o}C. Pandat Simulations, the software used to determine the phase change during solidification, indicated the eutectic phase began to form at this temperature. Since the eutectic silicon was modified by strontium, this procedure could alter the load rate. After the eutectic procedure, the load curve seemed similar to that of A380.1; at 60 seconds, the load of A380.1 modified with Sr reached 1406N, which was close to the value of A380.1 without the addition of Sr. In the derivative of load, the incipient crack rate for modified A380.1 was only 5N/s. Compared with the high incipient crack rate of 15N/s of unmodified A380.1 alloy, the addition of strontium reduced the occurrence of incipient cracks, implying a significant increase in the hot tearing resistance.

In analyzing the LVDT data, the most noticeable difference between modified and unmodified A380.1 was the value of linear displacement/contraction at 60 seconds. While A380.1 without Sr had a 1.09mm linear displacement, there was only a 0.85mm

change for the modified A380.1. According to M.M. Haque's paper, in aluminum-silicon alloys, the addition of strontium can slightly decrease the density [18]. As the density is reduced, the volume is expanded. In this case, the smaller contraction of modified A380.1 can be explained from this aspect: as the Sr addition reduced the density, the volume increased while the linear contraction decreased.

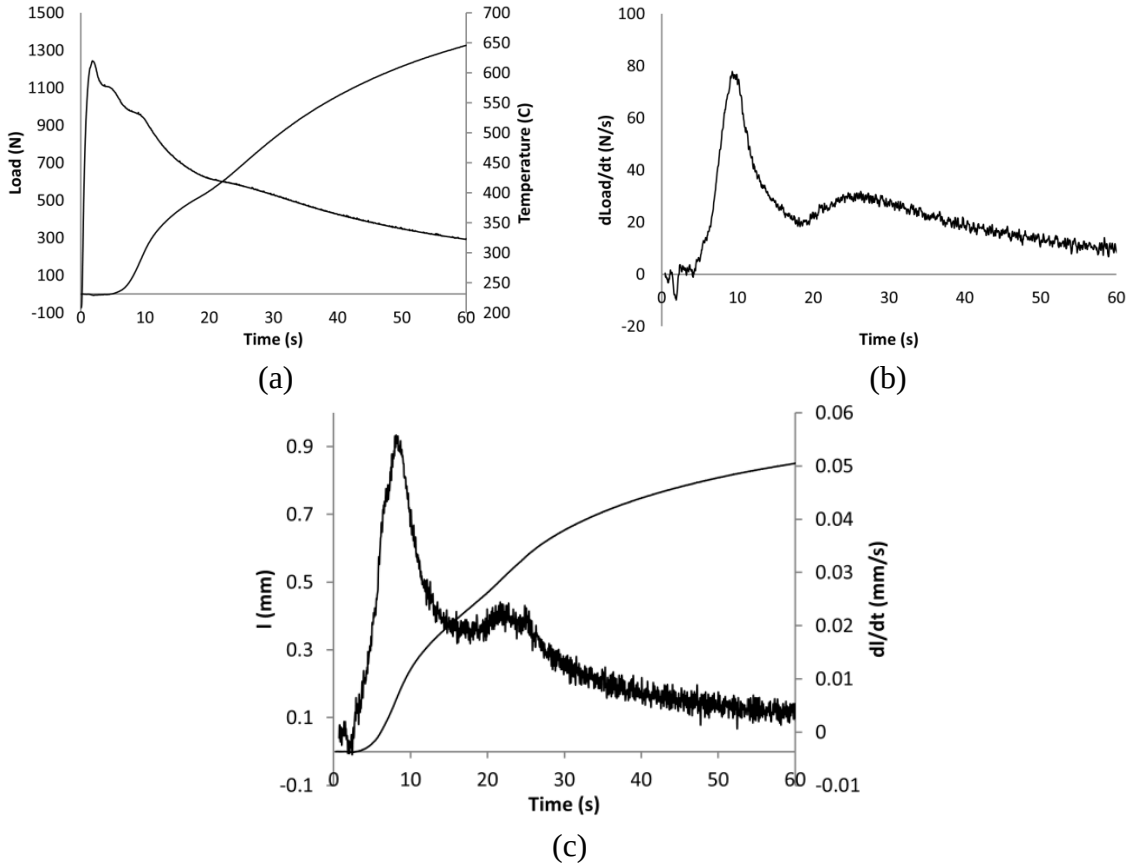

Figure 22: (a) Load development and temperature vs. time for A380.1 modified with strontium; (b) Derivative of load vs. time; (c) Displacement and its derivative vs. time

Table 9: Contraction force and linear displacement measurement data

Alloy	Incipient crack loading rate (N/s)	Maximum loading rate (N/s)	Load @ 60 seconds (N)	Maximum displacement rate (mm/s)	Displacement @ 60 seconds (mm)
Unmodified A380.1	15	62	1400	0.052	1.09
Modified A380.1	5	76	1406	0.054	0.85

5.3.2 Mosaic optical micrograph and microstructure

Figure 23 shows that no cracks were found in either the modified A380.1 or unmodified A380.1 alloys. Figure 24a illustrates that the microstructure of A380.1 without addition of strontium consists of α-aluminum and acicular divorced eutectic silicon. However, most of the eutectic silicon particles in Figure 24b for A380.1 modified with strontium were fully fine fibrous or globular-like. The mechanism of the improved property of Sr-modified Al-Si alloys can be explained as the Twin Plane Re-entrant Edge (TPRE) [27]. During solidification, the strontium atoms are absorbed onto the surface steps and kinks. A new atomic layer attempts to grow around the strontium atoms. This behavior changes the sequence of the atomic layer and causes twinning in the silicon crystals.

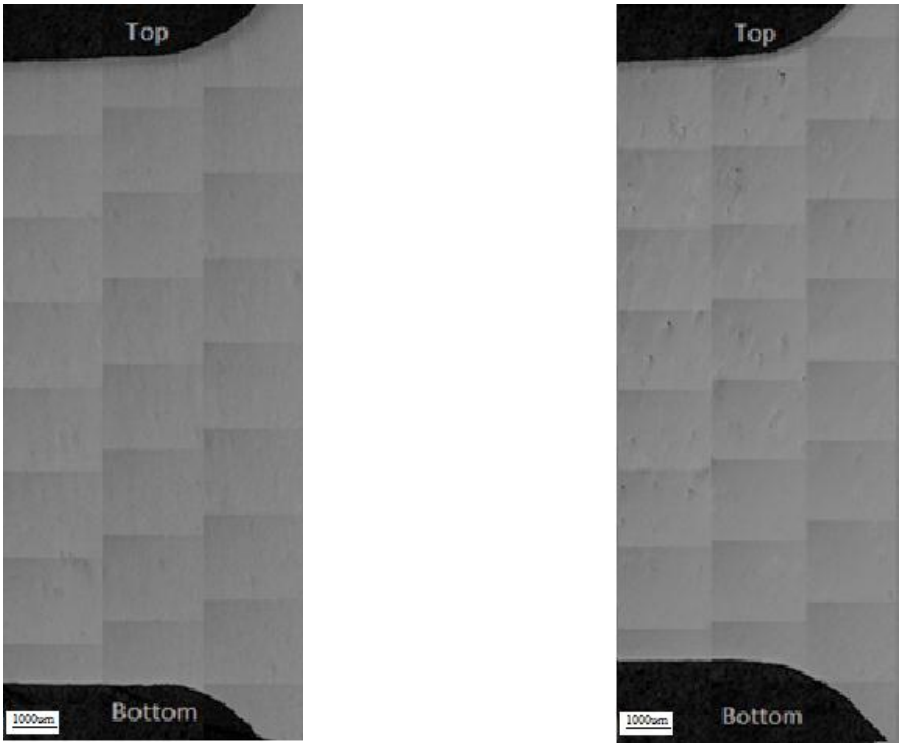

(a) (b)

Figure 23: (a) Mosaic optical micrograph showing the longitudinal cross section of the neck region of pure A380.1; (b) Mosaic micrograph in the neck region of A380.1 modified with Sr

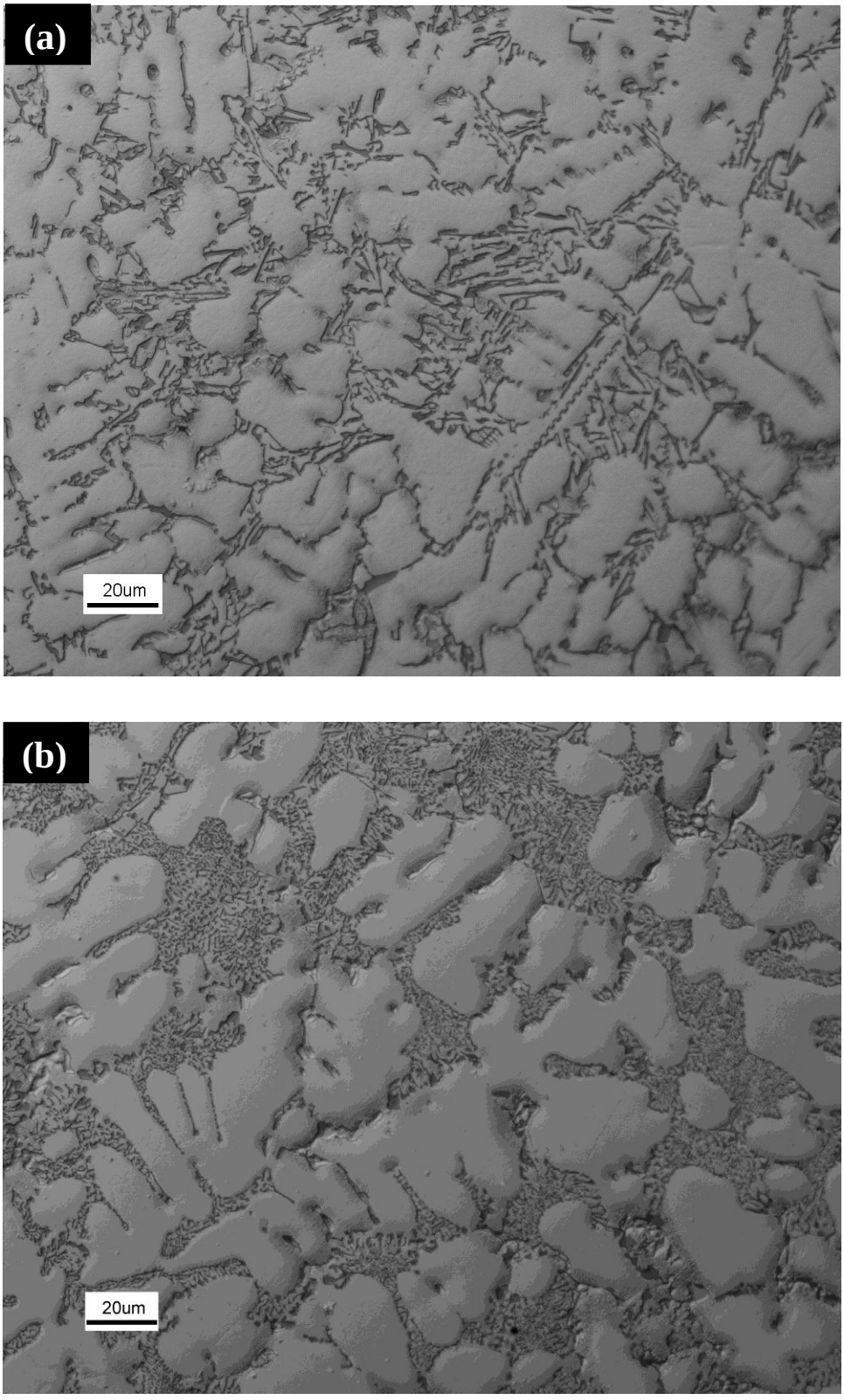

Figure 24: (a) Optical micrograph of pure A380.1; (b) Optical micrograph of A380.1 modified with Sr

5.4 Effect of oxides

The chemical compositions of A380.1 and A380.1 including oxides are given in Table 10. However, due to the limitation of characterization technique, the composition of oxygen cannot be presented here. In the later part of the oxides addition, other methods were used to prove the existence of oxygen and oxides in the alloy.

Table 10: Chemical composition of alloys A380.1 and A380.1 with added oxides (wt.%)

Alloy	Si	Fe	Cu	Mn	Mg	Ti	Ni	Zn	Sn
380	8.26	0.7	3.77	0.1	0.058	0.02	0.054	1.54	0.02
380+oxide	8.05	0.485	3.92	0.057	0.016	0.01	0.039	0.94	0.013

5.4.1 Load, displacement and temperature measurements

The load, temperature and displacement data recorded during solidification of A380.1 with added oxides are shown in Figure 25. The shapes of the load and LVDT curve for this alloy were very similar to that of A380.1. In this experiment, load started at 2 seconds and increased at the similar maximum loading rate of pure A380.1. At 60 seconds, the load and displacement were slightly lower than A380.1, indicating that the formation of cracks could reduce the value of load and displacement.

According to Table 11, the most distinguishable item in the load cell data was the incipient crack loading rate. For A380.1 including oxides this value reached 25N/s, which was much higher than 15N/s of pure A380.1. This indicated that at the early stage of solidification for A380.1 including oxides, more incipient cracks formed and needed more remaining liquid to refill the cracks. However, adding oxide inclusions into cast aluminum alloys can hinder the refilling of cracks during solidification by decreasing the fluidity of alloys [19, 20]. Consequently, cracks were more likely to be formed in the A380.1 alloy with added oxides. Based on this analysis, one can conclude that A380.1 with added oxides has a higher hot tearing tendency.

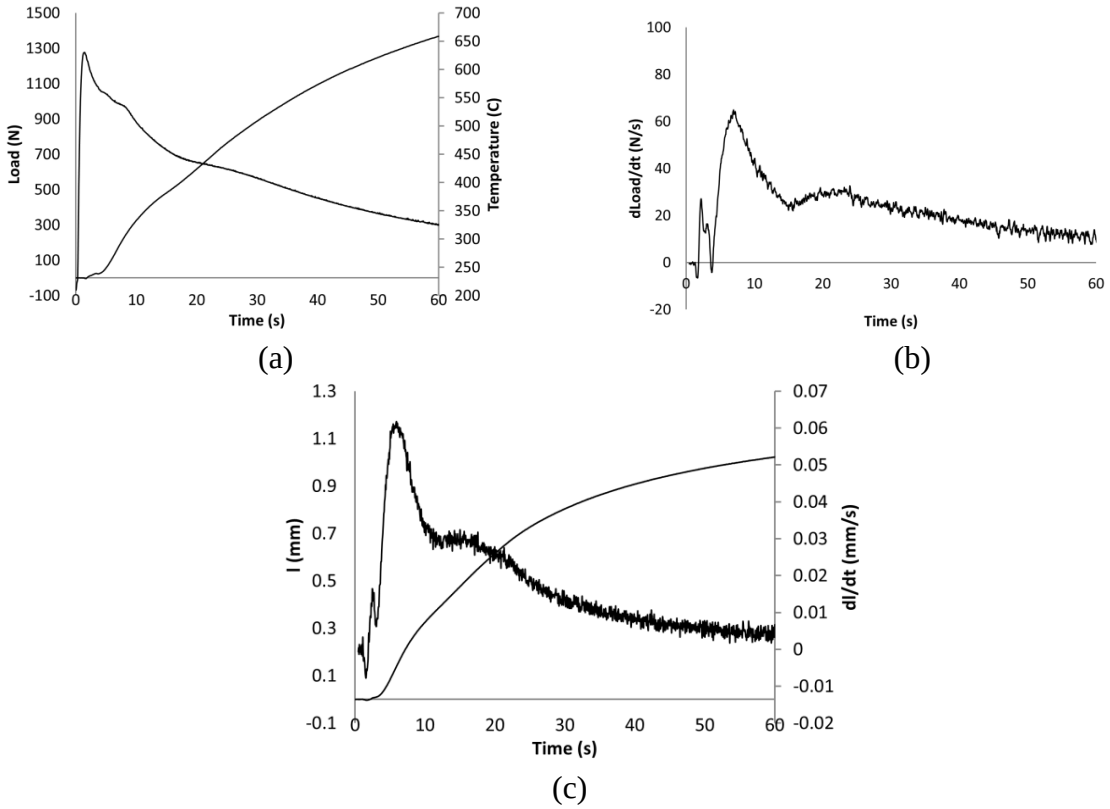

Figure 25: (a) Load development and temperature vs. time for A380.1 with added oxides; (b) Derivative of load vs. time; (c) Displacement and its derivative vs. time.

Table 11: Contraction force and linear displacement measurement data

Alloy	Incipient crack loading rate (N/s)	Maximum loading rate (N/s)	Load @ 60 seconds (N)	Maximum displacement rate (mm/s)	Displacement @ 60 seconds (mm)
A380.1	15	62	1400	0.053	1.09
A380.1 added oxides	25	63	1368	0.059	1.04

5.4.2 Mosaic optical micrograph and microstructure

At the neck region, a fine crack was found on the surface of the cast (Figure 26a). After the sample was cut, ground and polished, the crack could be seen clearly (Figure 26c). The crack area was around 0.17mm^2. This crack started from the surface and grew into the internal part with the crack becoming smaller from the surface to the deeper section. In comparing this with the image (Figure 26b) of pure A380.1 in which no cracks are observed, one can conclude that oxides can apparently increase the hot tearing tendency for cast alloys.

In the optical micrograph (Figure 27b), many nonmetallic particle oxides (pointed out by circles and indicated by dark and irregular shapes) can be found in the matrix of A380.1 with added oxides compared to that of the pure A380.1 (Figure 27a).

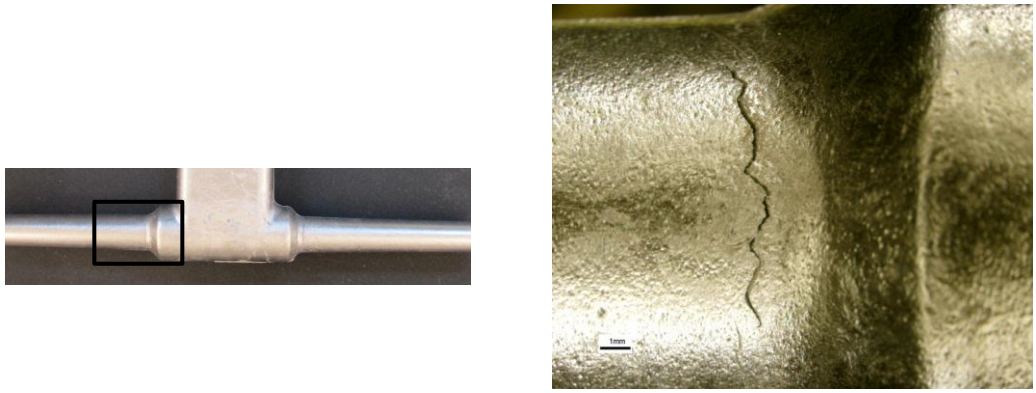

(a)

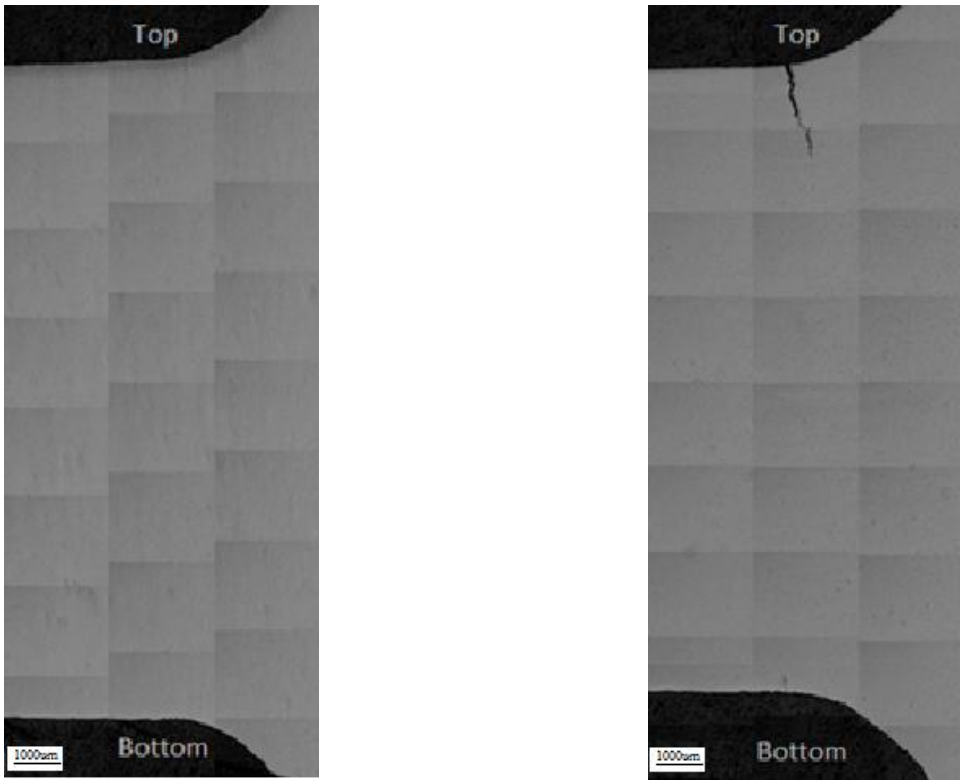

(b) (c)

Figure 26: (a) Photographs of the constrained casting showing cracking locations of A380.1 with added oxides; (b) Mosaic optical micrograph showing the longitudinal cross section of the neck region of pure A380.1; (c) Mosaic micrograph showing hot tears in the neck region of A380.1 with added oxide inclusion

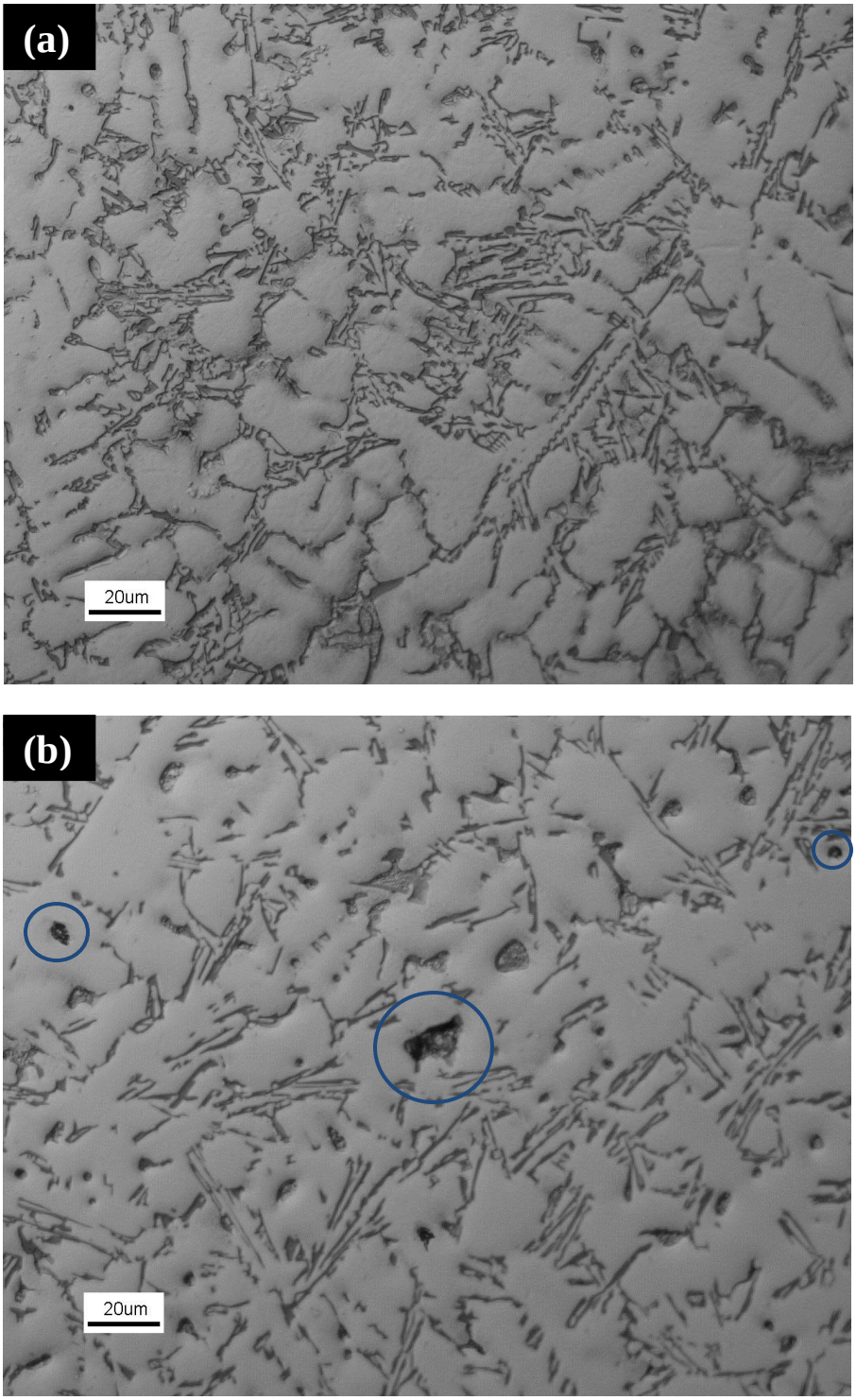

Figure 27: (a) Optical micrograph of pure A380.1; (b) Optical micrograph of A380.1 with added oxide inclusion. The circle points out the oxides.

5.4.3 SEM and EDX analysis

In order to determine the oxides' effects on the formation of cracks, SEM images and EDX spectrum were used to examine oxides along the crack at the neck region of sample alloy A380.1 with added oxides.

Three different areas were chosen to identify the existence of oxides. Figure 28 shows the SEM image of the crack and the selected areas. For each area, two spectra were measured and analzyed by EDX to acquire their chemical compositions.

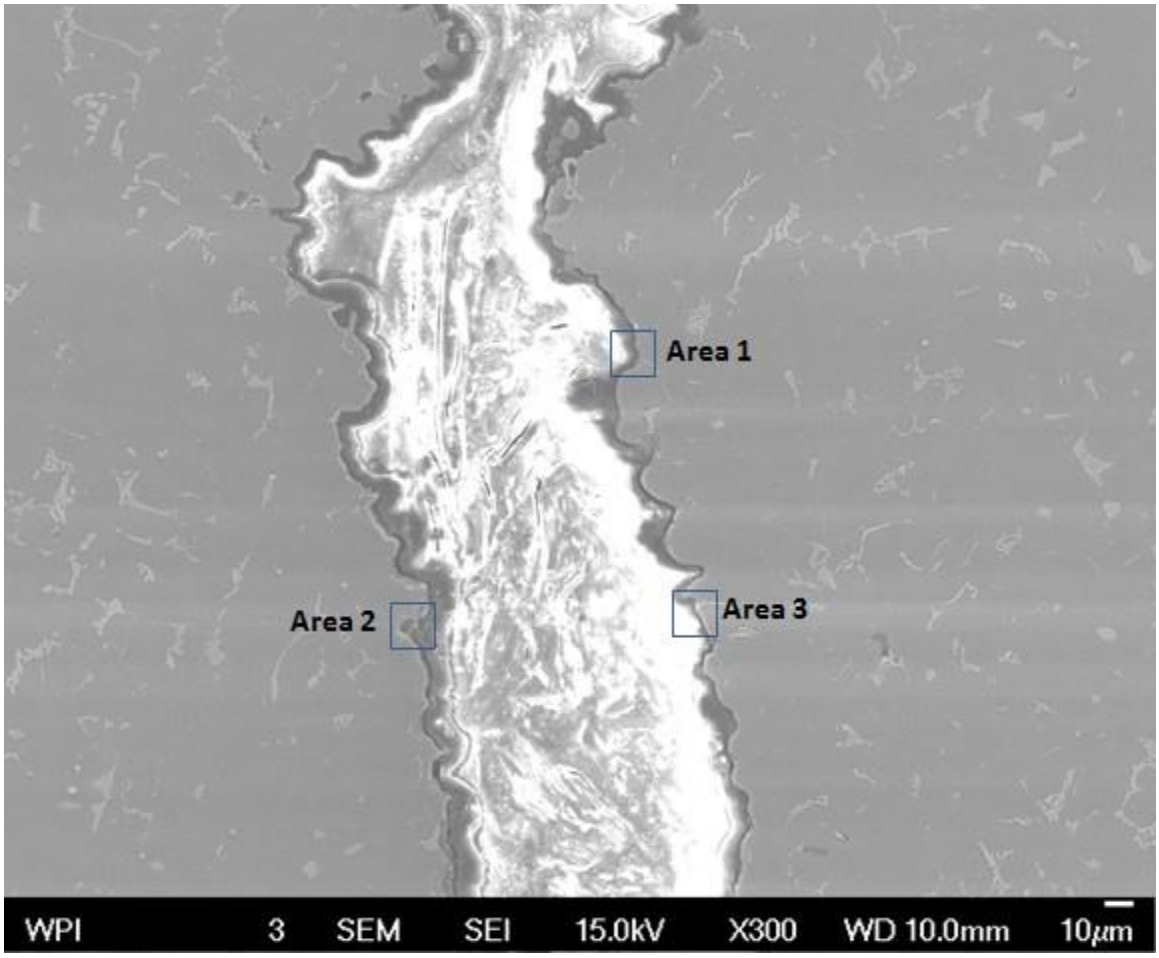

Figure 28: SEM image of the crack and areas analyzed in A380.1 with added oxides

In Area 1 of Figure 29, on the SEM image, the region for spectrum 1 was white and just along the crack. More Si, O and C were found in spectrum 1 than in spectrum 2, which indicated that SiO, SiC or Al_2O_3 may be formed at this location. It also validates the existence of oxides in the alloy.

In Area 2 (Figure 30), more Cu, Si, O, and C were found in spectrum 1 than in spectrum 2. So in spectrum 1, the sample may consist of a Cu phase and the oxides of Si, Cu or Al. For spectrum 2, no oxygen was detected, excluding the presence of oxides.

In Area 3 (Figure 31), spectrum 2 was taken from a white dot on the surface. Analysis indicated that the scanned area contained much more Cu and eutectic Si. At the same time, oxygen was also detected in spectrum 1. The presence of C is probably introduced by the addition of potatoes.

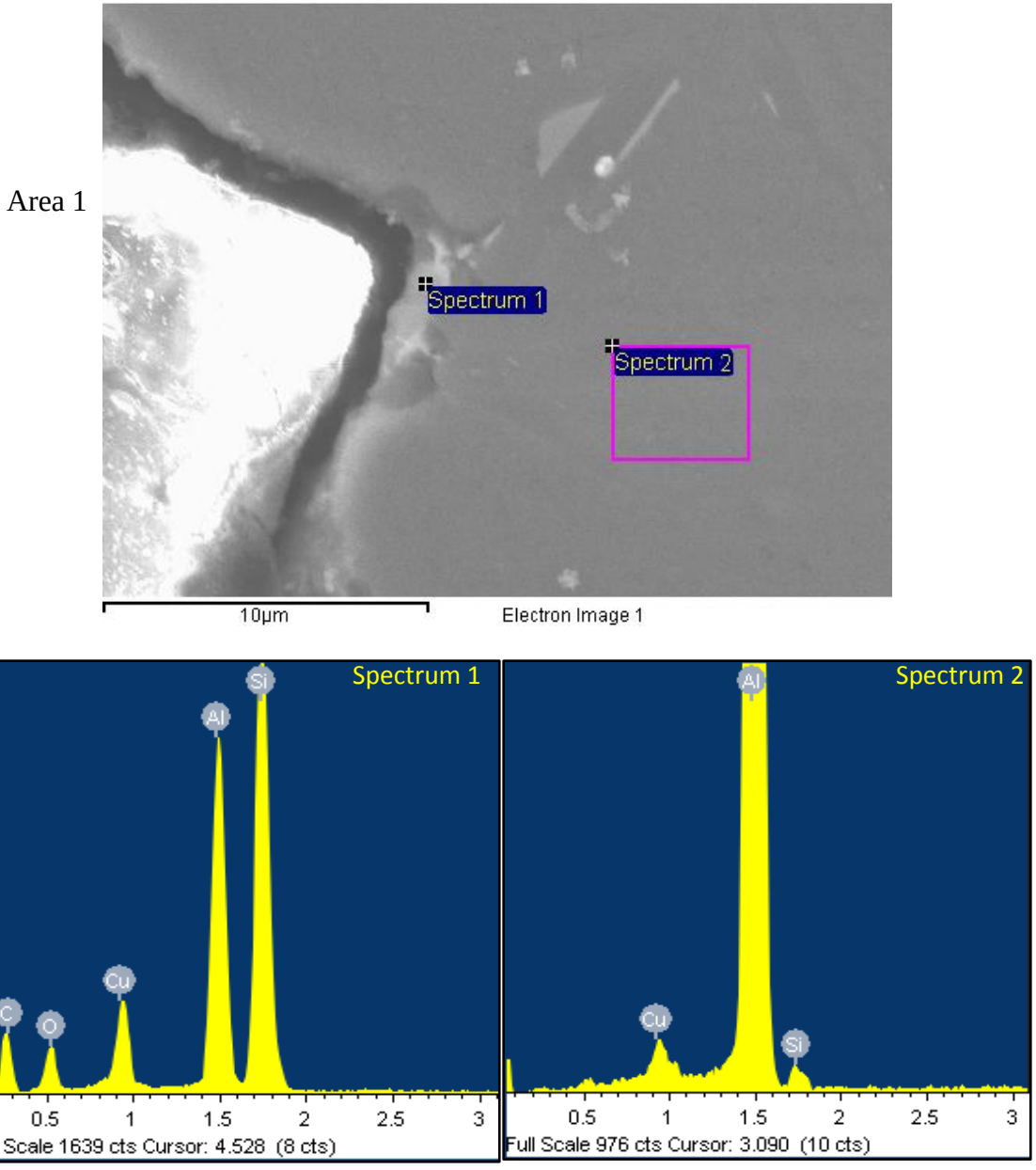

Figure 29: EDX report for Area 1

Area 2

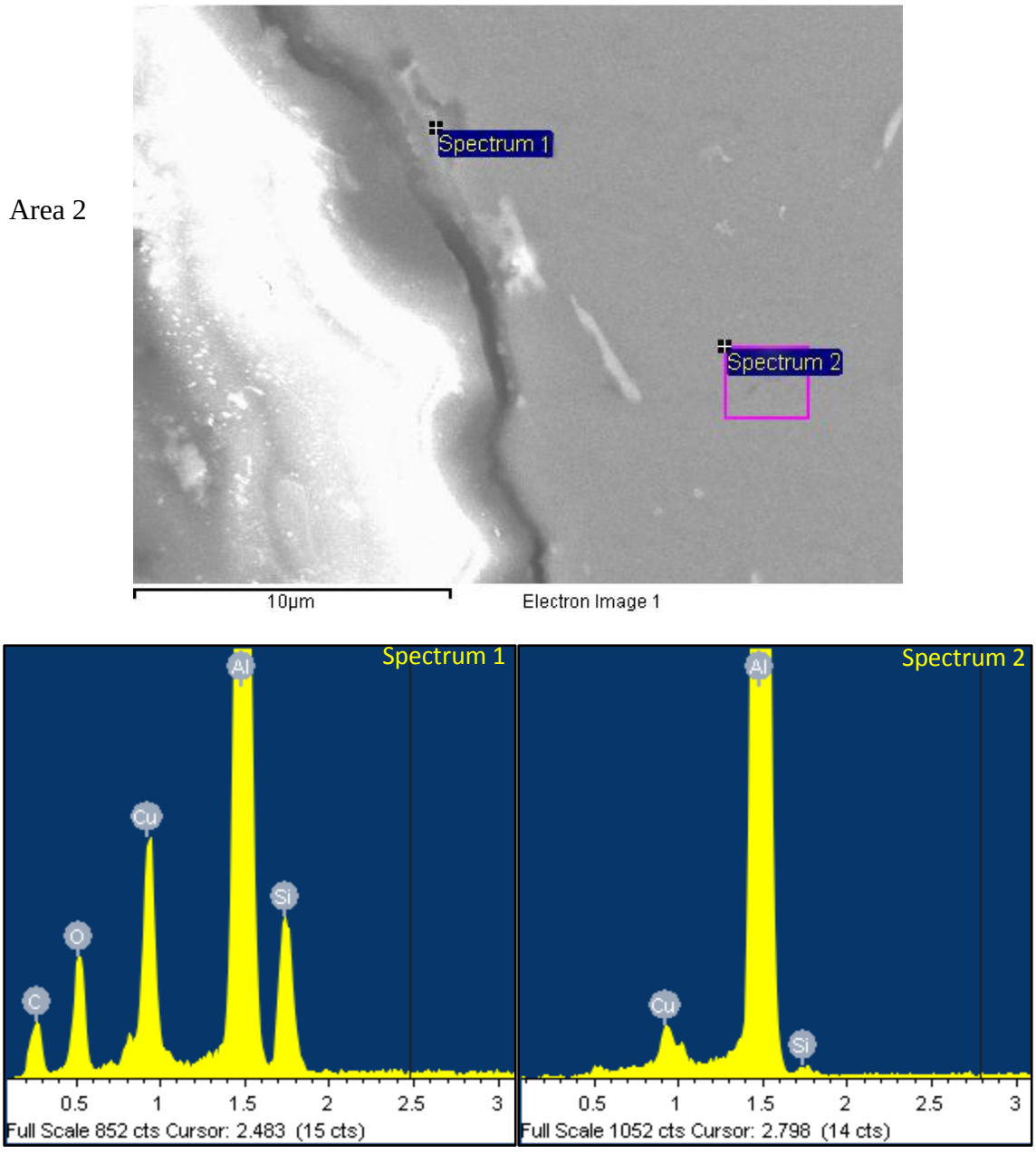

Figure 30: EDX report for Area 2

Area 3

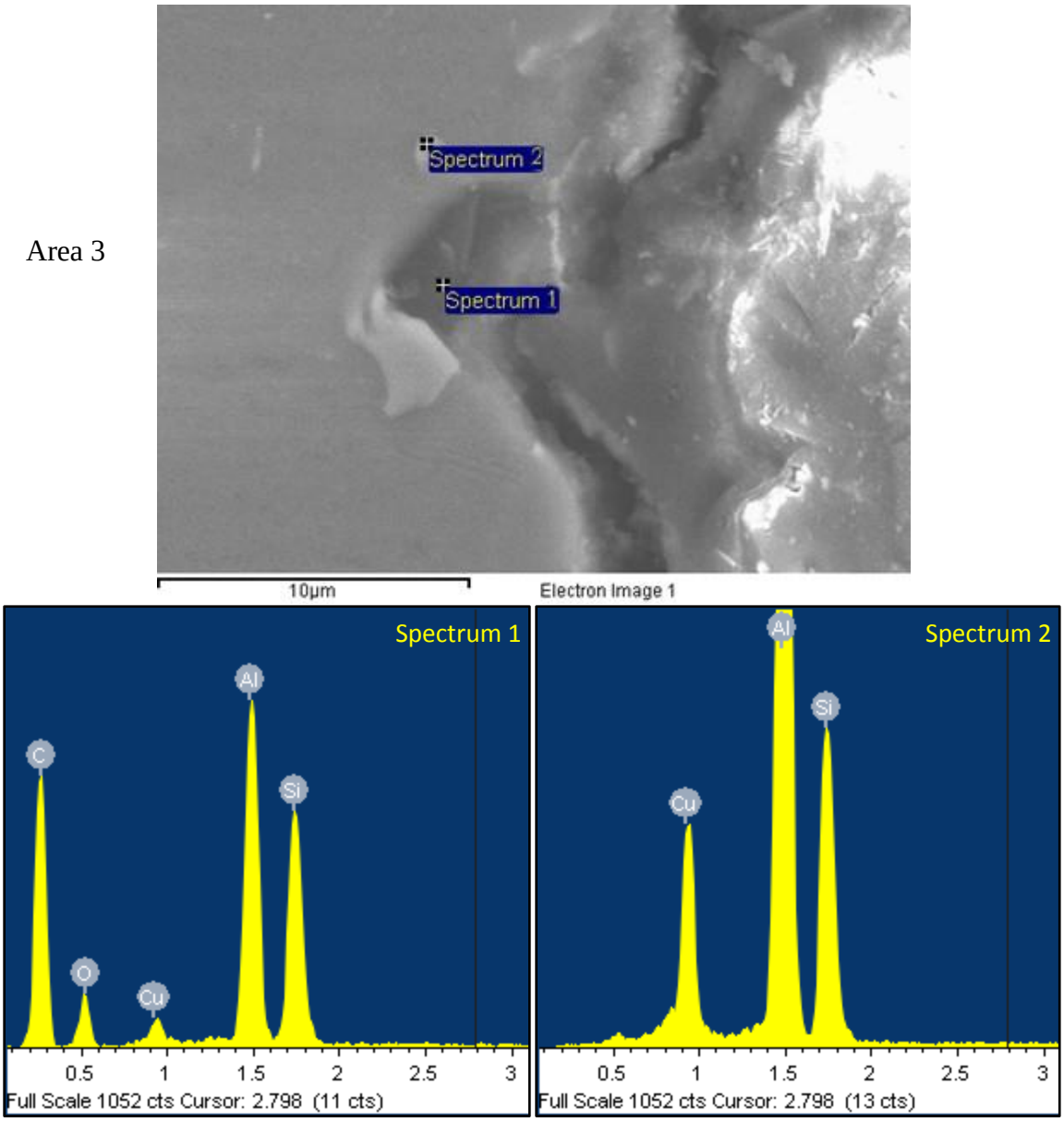

Figure 31: EDX report for Area 3

As shown in the SEM and EDX images, the existence of oxides in this alloy was confirmed (from Figure 29 to Figure 31). Since oxides are defects in casting [28], cracks might be generated around the oxides during solidification. Meanwhile, the addition of oxides could reduce the fluidity of alloys, which makes it hard for the remaining liquid to fill the incipient cracks at the early stage during solidification in casting. Then the remaining tiny cracks begin to propagate until solidification is completed. Many oxides were found along the cracks, which revealed the possibility that the presence of oxides was one of the factors increasing the hot tearing tendency.

5.5 New hot tearing index

Based on the results mentioned above, at 200^{o}C mold temperature, one can get a sequence of the hot tearing tendency for these alloys. In cast aluminum alloys, the hot tearing tendency from the lowest to the highest was based on the value of the incipient crack loading rate and the crack condition as explained in this sequence:

A380.1 modified with Sr < A390 < A380.1 < A380.1 with added oxides.

Li's [24] paper tested for hot tears in A356 and M206. For A356, no cracks were found, and the incipient crack loading rate was around 4N/s. For M206, there were large hot tears with a 12.4mm^2 crack area. Also no obvious incipient crack loading rate could be detected in M206. Combining Li's information with the data contained in this thesis, one can establish a new sequence of hot tearing tendency for cast aluminum alloys:

A356 < A380.1 modified with Sr < A390 < A380.1 < A380.1 with added oxides < M206.

In wrought aluminum alloys, the hot tearing tendency sequence is as follows:

7075 < 6061.

Large cracks could be detected after solidification for 6061 and 7075. However, no incipient crack loading rate can be seen from the load curve for both wrought alloys.

In combining the results of tests performed on M206, 6061 and 7075, one can conclude that with large hot tearing cracks, it seems difficult to determine the incipient crack loading rate. This can be explained by the fact that there was no large fluctuation on the loading rate at the early stage of solidification, indicating that the remaining liquid could not fill the incipient cracks. So with the aid of this new method of testing for hot tearing, one can set an index involving two parts: no-crack and large-crack. The middle line of the index is marked by a tiny crack with high incipient crack loading rate, as founded in A380.1 with added oxides.

For the no-crack part of the index, by normalizing the incipient crack loading rate with a scale from 1 to 5, one can calculate the hot tearing index for these alloys with a 0N/s incipient crack loading rate as the starting point (Table 12). Results are plotted in Figure 32.

Table 12: Incipient value for no-crack part

Alloy	Starting point	A356	A380.1+Sr	A390	A380.1	A380.1+oxides
Incipient crack loading rate (N/s)	0	4	5	10	15	25
Index	1	1.64	1.8	2.6	3.4	5

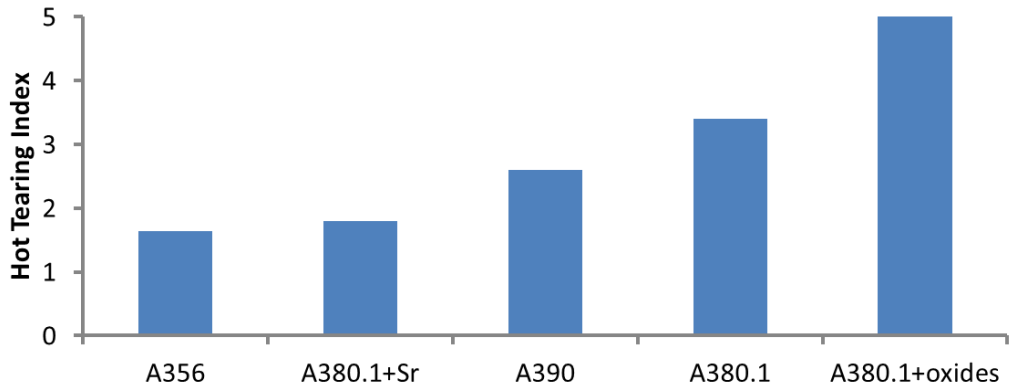

Figure 32: Hot tearing index for different alloys in the no-crack part

As for the large-crack part, the crack area was recognized as the reference for hot tearing. For 7075, around one-third of the neck region was still connected immediately after solidification. So 7075's crack area should be smaller than that of M206 (Figure 33 and Table 13).

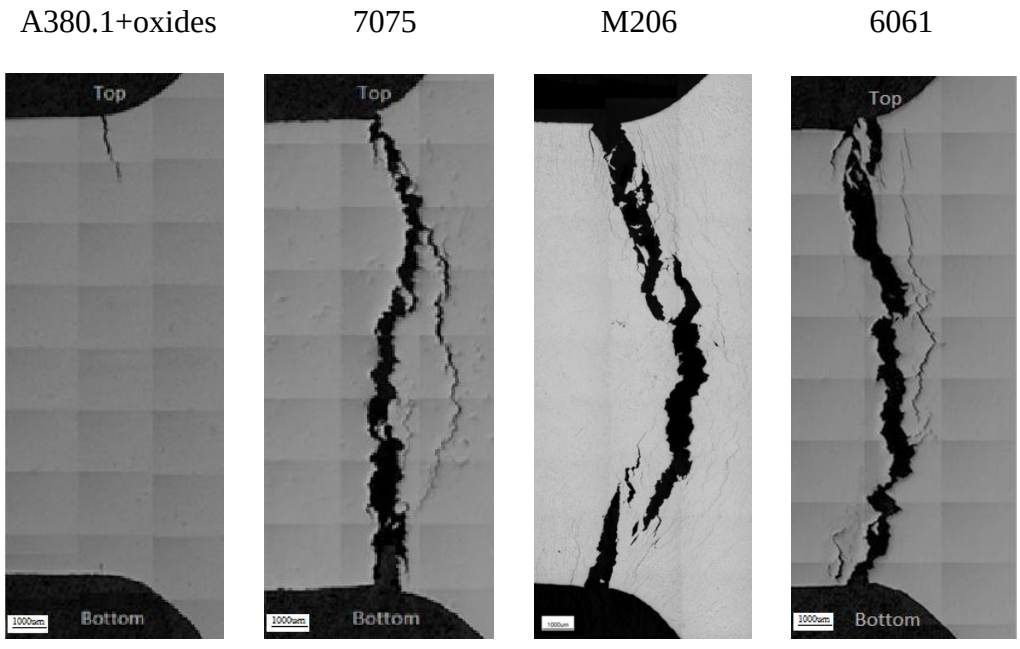

Figure 33: Crack images for A380.1+oxides, 7075, M206 [6], and 6061.

Table 13: Crack area of different alloys

Alloy	A380.1 + oxides	7075	M206	6061
Crack area (mm^2)	0.17	9.3	12.4	13.6

The derivative of load curves for A380.1, M206 and 6061 (Figure 34a, c, and d) show that the loading rate rapidly hit the maximum point (Rm) and then began to decrease to a certain value (Rd); subsequently, the rate started to increase once again. All these took place during 10-15 seconds. So, by comparing how the rate (S) decreased from Rm to Rd for the three alloys, one can establish the hot tearing index for the alloys represented in the large-crack part.

For 7075 (Figure 34b), no obvious increase could be seen after the decrease, so the rate at 15 seconds was selected as the Rd for comparison purposes. Normalizing the speed in using the scale of 5-10 establishes the index shown in Table 14. The hot tearing index for the large-crack part is plotted in Figure 35.

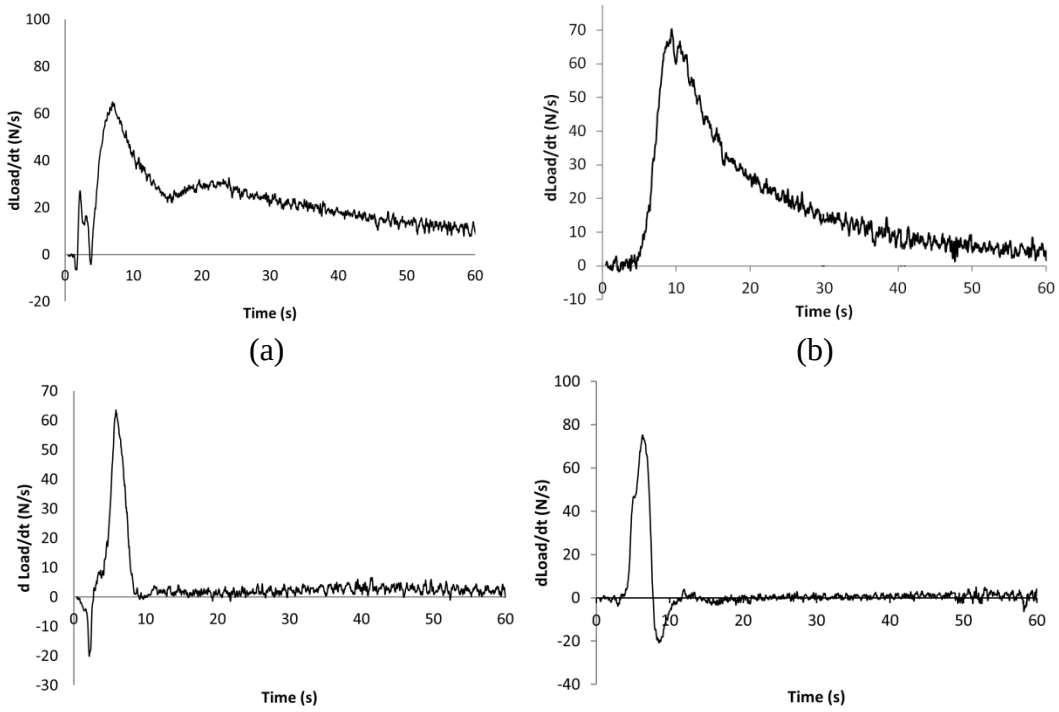

Figure 34: Derivative of load vs. time: (a)A380.+oxides, (b)7075, (c)M206 [24], (d)6061.

Table 14: Index value for large-crack part

Alloy	A380.1+oxides	7075	M206	6061
Rm (N/s)	63	72	62	74
Rd (N/s)	27	31	0	-20
Time (s)	9.2	5.4	3.3	2.25
S (N/s^2)	3.9	7.6	18.8	41.7
Index	5	5.5	7.0	10

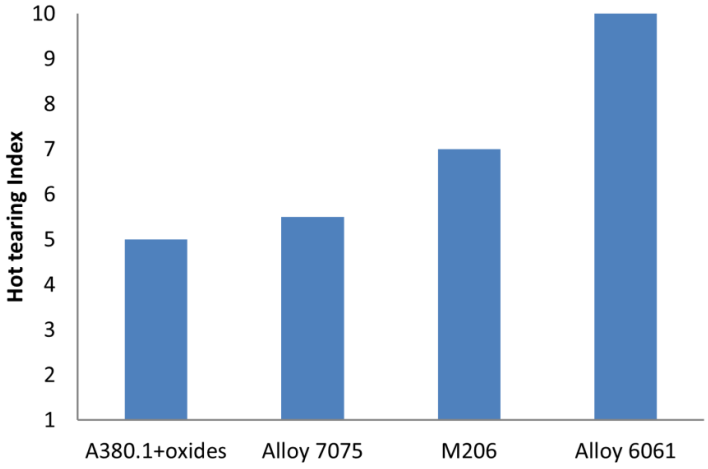

Figure 35: Hot tearing index for different alloys in the large-crack part

A complete diagram combining the two parts of the hot tearing index appears in Figure 36. A high value in the index indicates a high hot tearing tendency. At the same time, it is obvious that this new method of testing for hot tearing is effective for evaluating the hot tearing of alloys without cracks after solidification.

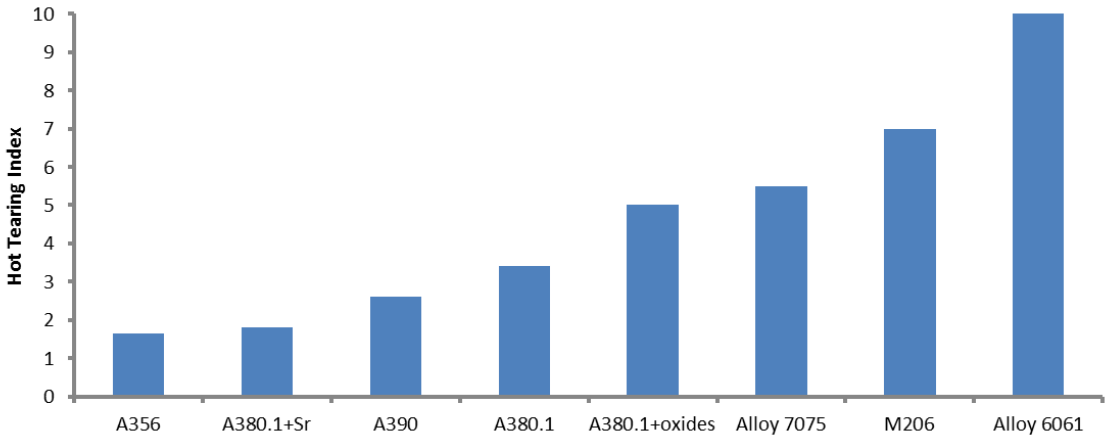

Figure 36: Hot tearing index for different alloys

6. Conclusions

(1) With a higher silicon composition, A390 contracted less than A380.1. There were no cracks found for either alloy. Additionally, the incipient crack loading rate of A390 was 10N/s, lower than 15N/s of A380.1, indicating more incipient cracks were formed at the early stage of solidification in A380.1. Therefore, hypoeutectic alloy A380.1 demonstrated a higher inclination towards hot tearing than hypereutectic alloy A390.

(2) There were no obvious incipient crack loading rates for 6061 and 7075 because the poor fluidity made it hard for the remaining liquid to fill the incipient cracks. A rapid drop of the data was detected for 6061, suggesting the occurrence of severe hot tears. Large cracks were found in both wrought aluminum alloys 6061 and 7075. Since the load and displacement changes of 6061 were more dramatic than in 7075, it was easier for 6061 to form hot tears during solidification. As shown in the fractograph, 6061 had larger dendrites with a clear directional property; many tiny stretched slices can be seen on 7075's hot tearing surface, which could be attributed largely to the remaining liquid attempting to fill the incipient cracks. Although the filling was not completed in the end, these slices represented the lower hot tearing tendency of 7075 than that of 6061.

(3) To modify the eutectic silicon from acicular divorced type to fully fine fibrous or globular-like shape, 0.03 wt.% strontium was added into A380.1. The addition of Sr may effectively decrease the hot tearing tendency by reducing the incipient crack loading rate from 15N/s to 4N/s. A convex on the loading curve occurring around 10-20 seconds for A380.1 modified with strontium was caused by the formation of eutectic.

(4) Introduction of oxide impurities gave rise to tiny cracks in A380.1 at the neck region. The incipient crack loading rate for A380.1 with oxides increased to 25N/s. When examining the microstructure, one could detect many oxides along the cracks. All this evidence proves that adding oxides into A380.1 increases the hot tearing tendency.

(5) By dividing the test alloys into two categories, no-crack and large-crack, a new hot tearing index is established in the present work using the Instrumented Constrained Rod Mold. The middle line of the index is marked by a tiny crack with high incipient crack loading rate as found in A380.1 with added oxides. The index ranges from 1 to 10, with the higher value indicating a higher hot tearing tendency.

7. References

[1] X. Yan, J.C. Lin, “Prediction of Hot Tearing Tendency for Multicomponent Aluminum Alloys”, Metallurgical and Materials Transactions B, vol.37B, pp.913-918, (2006).

[2] S. Lin, C. ALIRAVCI, M.O. PEKGULERYUZ, “Hot-Tear Susceptibility of Aluminum Wrought Alloys and the Effect of Grain Refining”, Metallurgical and Materials Transactions A, vol. 38, pp.1056-1068, (2007).

[3] S. Li, D. Apelian, “Hot Tearing of Aluminum Alloys – A Critical Literature Review”, International Journal of Metalcasting, vol. 5, I 1, pp.23-40, (2011).

[4] D. G. Eskin, Suyitno, L. Katgerman, "Mechanical Properties in the Semi-Solid Sate and Hot Tearing of Aluminum Alloys," Progress in Materials Science, vol. 49, pp. 629-711, (2004).

[5] S. Li, K. Sadayappan, D. Apelian, “Characterization of Hot Tearing in Al Cast Alloys: Methodology and Procedures”, International Journal of Cast Metals Research, vol. 24, No. 2, pp.88-95(8), (2011).

[6] S. Li, K. Sadayappan, D. Apelian, “Hot tearing in Cast Aluminum Alloys”, Materials Science Forum, vol.690, pp.355-358, (2011).

[7] Mahmoud F. Hafiz, Toshiro Kobayashi, “Mechanical properties of modified and nonmodified eutectic Al-Si alloys”, Journal of Japan Institute of Light Metals, vol.44, Issue 1, pp.28-34, (1994)

[8] Sathyapal Hegde, K Narayan Prabhu, “Modification of eutectic silicon in Al–Si alloys”, Journal of Materials Science, vol.43, Issue 9, pp.3009-3027, (2008).

[9] E. Parshizfard, S.G. Shabestari, “An investigation on the microstructural evolution and mechanical properties of A380 aluminum alloy during SIMA process”, Journal of Alloys and Compounds, vol.509, Issue 40, pp.9654-9658, (2011)

[10] Yücel Birol, “Cooling slope casting and thixoforming of hypereutectic A390 alloy”, Journal of Materials Processing Technology, vol.207, Issue 1-3, pp200-203, (2008)

[11] R.J. Arsenault, "The strengthening of aluminum alloy 6061 by fiber and platelet silicon carbide", Materials Science and Engineering, vol. 64, Issue 2, pp. 171-181, (1984).

[12] C.M. Cepeda-Jiménez , J.M. García-Infanta, O.A. Ruano, F. Carreño, "High strain rate superplasticity at intermediate temperatures of the Al 7075 alloy severely processed by equal channel angular pressing", Journal of Alloys and Compounds, vol.509, Issue 60, pp.9589-9597, (2011).

[13] C.M. Cepeda-Jiménez, J.M. García-Infanta, M. Pozuelo, et al. "Impact toughness improvement of high-strength aluminum alloy by intrinsic and extrinsic fracture mechanisms via hot roll bonding", Scripta Materialia, vol.61, pp.407-410, (2009).

[14] L. Lu, A.K. Dahle, "Effect of Combined Additions of Sr and AlTiB Grain Refiners in Hypoeutectic Al-Si Foundry Alloys", Materials Science & Engineering A, vol. 435-436, pp.288-296, (2006)

[15] J.A. García-Hinojosa, C.R. González, G.M. González, Y. Houbaert, "Structure and Properties of Al-7Si-Ni and Al-7Si-Cu Cast Alloys Nonmodified and Modified with Sr", Journal of Materials Processing Technology, vol.143-144, pp.306-310, (2003).

[16] A. Razaghiana, M. Emamyb, A.A. Najimib, S.H. Seyed Ebrahimib, " Sr Effect on the Microstructure and Tensile Properties of A357 Aluminum Alloy and Al2O3/SiC-A357 Cast Composites", Materials Characterization, vol.60, pp.1361-1369, (2009).

[17] M. Garat, G.Laslaz, S. Jacob, et al., AFS Trans. 100 (1992) 821.

[18] M.M. Haque, "Effects of Strontium on the Structure and Properties of Aluminium-Silicon Alloys", Journal of Materials Processing Technology, vol.55, pp.193-198, (1995).

[19] Young-Dong Kwon, Zin-Hyoung Lee, "The effect of grain refining and oxide inclusion on the fluidity of Al/4.5Cu/0.6Mn and A356 alloys", Materials Science and Engineering A, vol.360, pp.372-376, (2003).

[20] M. Di. Sabatino, L. Arnberg, S. Rørvik, A. Prestmo, "The influence of oxide inclusions on the fluidity of Al–7 wt.%Si alloy", Materials Science and Engineering A, vol.413-414, pp.272-276, (2005).

[21] C. Nyahumna, N.R. Green, J. Campbell, AFS Trans. vol.106, pp.215–223, (1998).

[22] X. Dai, X. Yang, J. Campbell, J. Wood, Materials Science and Engineering A vol.354, pp.315–325, (2003).

[23] J. Campbell, “Thin wall castings”, Materials Science and Technology, vol.4, Number 3, pp.194-204, (1988)

[24] S, Li, “Hot Tearing in Cast Aluminum Alloys: Measures and Effects of Process Variables”, Ph.D, Worcester Polytechnic Institute, (2010).

[25] Mats Johnsson, “Grain refinement of aluminum studied by use of a thermal analytical technique”, Thermochimica Acta, vol.256, pp.107-121, (1995)

[26] M. Easton, H. Wang, J. Grandfield, D. StJohn, E. Sweet, "An Analysis of the Effect of Grain Refinement on the Hot Tearing of Aluminum Alloys," Materials Science Forum, vol. 28, pp. 224-229, (2004).

[27] D.R. Hamilton, R.G. Seindensticker, Journal of Applied Physics, vol.31, pp.1165, (1960).

[28] A Papworth, P Fox, “The disruption of oxide defects within aluminium alloy castings by the addition of bismuth”, Materials Letters, vol.35, Issue 3-4, pp.202-206, (1998)